Optophysiological analysis of pattern classification strategies in the zebrafish olfactory bulb

Inauguraldissertation

zur Erlangung der Würde eines Doktors der Philosophie
vorgelegt der
Philosophisch-Naturwissenschaftlichen Fakultät
der Universität Basel
von

Jörn Niessing

aus Marburg an der Lahn, Deutschland

Basel, 2012

creative commons

Namensnennung-Keine kommerzielle Nutzung-Keine Bearbeitung 2.5 Schweiz

---

Sie dürfen:

das Werk vervielfältigen, verbreiten und öffentlich zugänglich machen

Zu den folgenden Bedingungen:

Namensnennung. Sie müssen den Namen des Autors/Rechteinhabers in der von ihm festgelegten Weise nennen (wodurch aber nicht der Eindruck entstehen darf, Sie oder die Nutzung des Werkes durch Sie würden entlohnt).

Keine kommerzielle Nutzung. Dieses Werk darf nicht für kommerzielle Zwecke verwendet werden.

Keine Bearbeitung. Dieses Werk darf nicht bearbeitet oder in anderer Weise verändert werden.

- Im Falle einer Verbreitung müssen Sie anderen die Lizenzbedingungen, unter welche dieses Werk fällt, mitteilen. Am Einfachsten ist es, einen Link auf diese Seite einzubinden.
- Jede der vorgenannten Bedingungen kann aufgehoben werden, sofern Sie die Einwilligung des Rechteinhabers dazu erhalten.
- Diese Lizenz lässt die Urheberpersönlichkeitsrechte unberührt.

Quelle: http://creativecommons.org/licenses/by-nc-nd/2.5/ch/ Datum: 3.4.2009

Genehmigt von der Philosophisch-Naturwissenschaftlichen Fakultät auf Antrag von:

PD Dr. Rainer W. Friedrich
(Dissertationsleiter)

Prof. Dr. Andreas Lüthi
(Korreferent)

Prof. Dr. Silvia Arber
(Fakultätsverantwortliche)

Basel, den 02. März 2010

Prof. Dr. Eberhard Parlow
(Dekan)

Erklaerung:

Diese Arbeit wurde am Friedrich Miescher Institut für Biomedizinische Forschung in Basel, Schweiz unter der Anleitung von PD Dr. Rainer W. Friedrich angefertigt. Alle Experimente die dieser Arbeit zugrunde liegen wurden von Jörn Niessing durchgeführt. Die Daten wurden zum größten Teil von Jörn Niessing unter Beteiligung von Rainer W. Friedrich (Abb. 12, Abb. 16 a, Abb. 17, Abb 21a) analysiert. Das Manuskript welches dieser Dissertationsschrift abschnittsweise zugrunde liegt wurde von Jörn Niessing unter Beteiligung von Rainer W. Friedrich verfasst.

Abbreviations

Ala	alanine
Arg	arginine
BA	bile acid
BABTA	1,2-bis(o-aminophenoxy)ethane-N,N,N',N'-tetraacetic acid
Ca^{2+}	calcium
CV_{rep}	mean coefficient of variations of responses evoked by repeated applications of the same odor
Dp	dorsal telencephalon
GC	granule cell
HuC-YC	yellow cameleon fluorescent protein expressed under the Huc-promotor
His	histidine
Lys	lysine
M	molar
MC	mitral cell
Met	methionine
mM	millimolar
ms	millisecond
OB	olfactory bulb
ORN	olfactory receptor neurons
PC	principal component
PG	periglomerular cell
Phe	phenylalanine

rhod-2-AM	rhodamine-2- acetoxymethyl
s	second
SD/s.d.	Standard deviation
TDCa imaging	temporally deconvolved calcium imaging
Trp	tryptophan
Tyr	tyrosine
µl	microliter
µm	micrometer

Abstract

Classification of overlapping activity patterns is a common problem for sensory systems. For a robust representation of sensory stimuli, neuronal circuits should generalize over input patterns reflecting variations of the same stimulus but separate patterns representing different stimuli, even if they are highly overlapping. In the olfactory bulb (OB), input patterns evoked by related, yet distinct, odors are often highly overlapping but perceived as a different stimulus. Consistent with this observation, overlapping input patterns evoked by different odors become decorrelated at the level of OB output neurons, the mitral cells. Input patterns evoked by different concentrations of the same odor, on the other hand, can be quite different but are usually perceived as the same odor quality. To obtain insights into the principles underlying pattern classification in the OB, I measured activity patterns evoked by different stimulus concentrations across mitral cells using temporally deconvolved 2-photon calcium imaging in zebrafish. In addition, I morphed one stimulus into another by continuously changing their ratio in a binary mixture to examine the transition between representations of similar and non-similar stimuli. The intensity, time course and distribution of mitral cell response patterns changed substantially when odor concentration was varied. Nevertheless, response patterns across the population of mitral cells maintained a high correlation over a substantial concentration range. OB output activity patterns therefore retain concentration-invariant components and generalize over different odor concentrations. Morphing of similar and dissimilar stimuli, in contrast, resulted in abrupt transitions between two or three discrete representations, respectively. These transitions were not caused by shifts in the global network state but mediated by coordinated response changes among small neuronal ensembles. These results indicate that the olfactory bulb classifies input patterns into distinct output patterns in an attractor-like fashion.

Introduction

Pattern classification: A common problem for sensory systems

The brain is confronted with a continuous stream of sensory information about the external world coming through different sensory modalities. Within each individual modality the first neural representation of the sensory stimulus is evoked in the primary sensory organs. This initial representation is transmitted to higher brain areas through a hierarchy of neuronal processing stages, thereby becoming increasingly more abstract. Since sensory information is the basis for higher cognitive tasks such as object recognition, working memory and decision making, the brain has to classify sensory stimulus representations into meaningful categories. The most basic form of pattern classification involves the categorization of input representations evoked by different sensory stimuli. This segmentation is an important computation for stimuli that are highly similar in their neural representations such as chemically similar odors in the olfactory system or similar faces in the visual system. This is a particular problem since overlapping input representations can arise from identical stimuli, as well as from different stimuli which are highly related. Consequently, the only basis for a correct segmentation of overlapping input representations are differences between the input patterns. These input differences are usually small and can arise either from real differences between non-identical stimuli, or from differences in the conditions of stimulus presentation of identical stimuli, such as changes in stimulus intensity or background noise. However, sensory systems usually are able to perform a correct pattern classification on the basis of very small input differences by generalizing over input variations evoked by identical stimuli presented under different conditions and separating inputs evoked by related, yet different, stimuli. For example, we are able to correctly identify the same face by generalizing over changes in stimulus condition such as differences in lighting, perspective or distance. In contrast, we usually can well separate different faces from each other, even though if they highly look alike. Likewise, animals can discriminate between related odors in an olfactory scene even if they differ only minimally in chemical structure (Valentincic, Kralj et al. 2000). In contrast, odors presented at different concentrations or in the presence

of different background odors are usually recognized as the same stimulus (Krone, Mannel et al. 2001; Abraham, Spors et al. 2004). Hence, also the olfactory system separates some sensory input differences but generalizes over others, thereby creating stimulus-specific perceptions that are robust against variations in intensity and noise. This balance between the separation and generalization of neuronal representations is critical also for a wide variety of other tasks including working memory, decision making (Wang 2008), multistable perceptions (Leopold and Logothetis 1999; Parker and Krug 2003) or hippocampal remapping (Colgin, Moser et al. 2008). Nevertheless, the strategies and mechanisms employed by the brain to solve this problem are poorly understood.

Functional organization and pattern classification in the olfactory system

The olfactory bulb (OB) is a telencephalic structure and the first center of olfactory information processing in the brain (Fig. 1). Odors are first detected by about 100 - 200 (rodents: >1000) different G-protein coupled odorant receptors in the olfactory receptor neurons (ORNs) of the nasal epithelium (Firestein 2001).

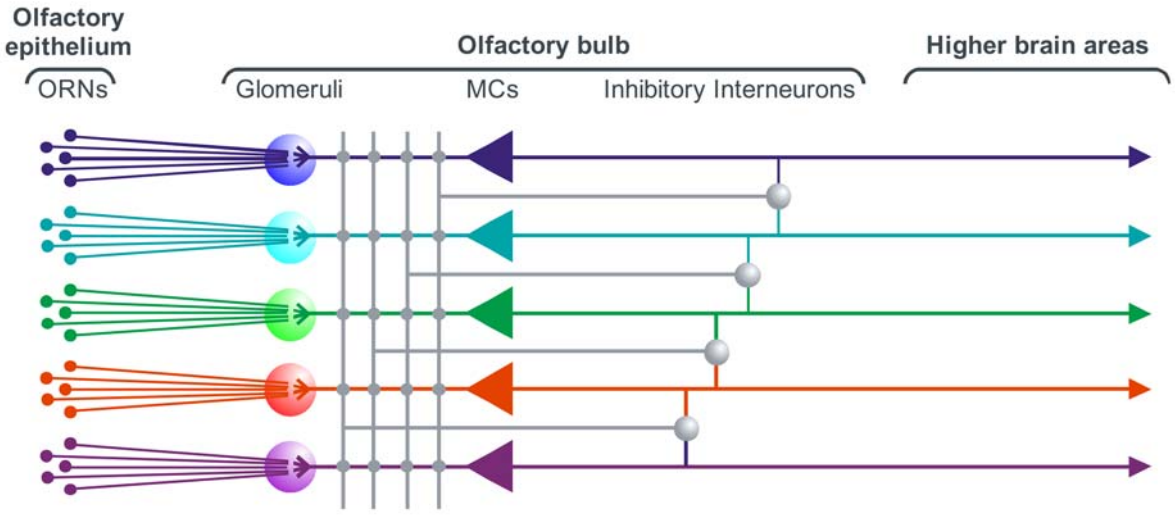

Figure 1 | **Illustration of the zebrafish olfactory system.** Olfactory receptor neurons (ORNs, left) make synaptic contacts with mitral cell (MC) dendrites within the glomeruli. Each glomerulus receives convergent input from ORNs expressing the same odorant receptor. MCs are laterally and recurrently interconnected via inhibitory interneurons (periglomerular cells and granule cells).

ORN axons project to distinct spherical structures, the glomeruli, in the outer layer of the OB (Fig. 1). Each glomerulus receives convergent input from ORNs expressing the same odorant receptor (Malnic, Hirono et al. 1999) and each ORN expressing the same receptor project usually to only one or, at most, a few glomeruli (Ressler, Sullivan et al. 1994; Vassar, Chao et al. 1994; Mombaerts, Wang et al. 1996). Within the glomeruli, excitatory mitral cells (MC) as well as local inhibitory interneurons (periglomerular cells) receive the synaptic input from the ORNs (Satou 1990; Shipley and Ennis 1996). Individual MCs are connected to only one or a few glomeruli (Satou 1990; Dryer and Graziadei 1994), and convey the output of the olfactory bulb to different higher brain areas (Haberly and Price 1977; Haberly 2001). These axonal projections form the olfactory tract which diverges to multiple targets including piriform cortex, anterior olfactory cortex, entorhinal cortex, amygdala, olfactory tubercle and agranular insula (Finger 1975; von Bartheld, Meyer et al. 1984; Levine and Dethier 1985; Neville and Haberly 2004; Rink and Wullimann 2004; Wilson, Kadohisa et al. 2006). The deep layers of the OB contain numerous inhibitory granule cells (GC, Fig. 1) that form reciprocal and lateral connections with MCs (Satou 1990; Shipley and Ennis 1996). The OB therefore contains a network of MCs and interneurons that is characterized by widespread inhibitory interactions.

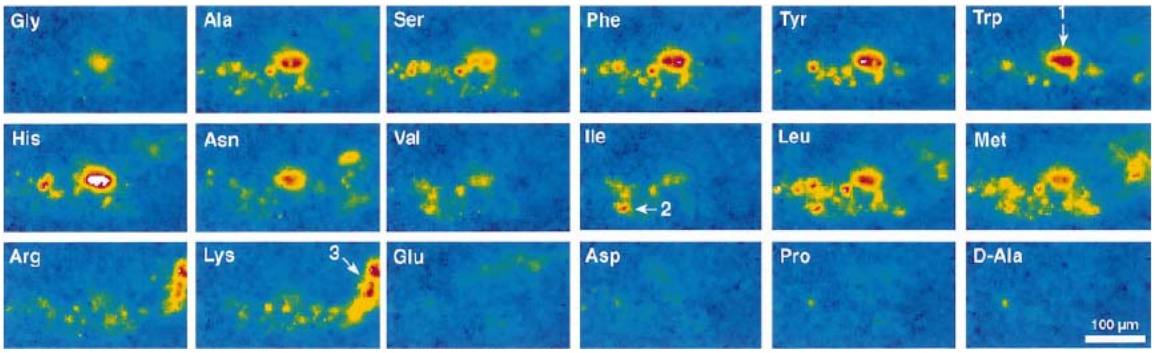

Figure 2 | Combinatorial glomerular input patterns evoked by 18 different amino acids in the OB. Activity patterns were measured by optical imaging with calcium-sensitive dyes (from Friedrich, Korsching, 1997).

Different odors evoke different combinatorial patterns of activity across the ORNs and glomeruli at the surface of the OB (Fig. 2) (Friedrich and Korsching 1997; Wachowiak, Denk et al. 2004). Glomerular activation maps are usually composed of large and distributed regions activated by primary molecular features (e.g. functional groups), while secondary molecular features (e.g. chain

length) are mapped in a more overlapping fashion within these regions (Fig. 2) (Friedrich and Korsching 1997; Friedrich and Korsching 1998; Uchida, Takahashi et al. 2000; Mori, Takahashi et al. 2006).

While glomerular input patterns are very different for chemically dissimilar odors (Fig. 2, compare Met and Arg), more similar odors evoke highly overlapping patterns (Fig. 2, e.g. compare Ala to Phe; Fig. 3, left). Experiments in zebrafish revealed that similarities of input patterns evoked by similar odors are also reflected in the initial activity pattern evoked in the population of the projection neurons of the OB, the mitral cells (Fig. 3, right). However, within the first second after response onset the overlap becomes decorrelated by odor specific sparsening of the MC population activity pattern. This computation generates output patterns across the output neurons that are more distinct than their inputs (Fig. 3, right) (Friedrich and Laurent 2001; Friedrich, Habermann et al. 2004; Yaksi, Judkewitz et al. 2007). Hence, neuronal circuits in the OB amplify small differences between glomerular input representations of similar odors, consistent with the ability of animals to make fine odor discriminations (Abraham, Spors et al. 2004; Valentincic, Miklavc et al. 2005). However, input patterns can also change substantially with the concentration of an odor (Fig. 4) (Friedrich and Korsching 1997; Johnson and Leon 2000; Bozza, McGann et al. 2004). In zebrafish and mice, a 10-fold increase in odor concentration can more than

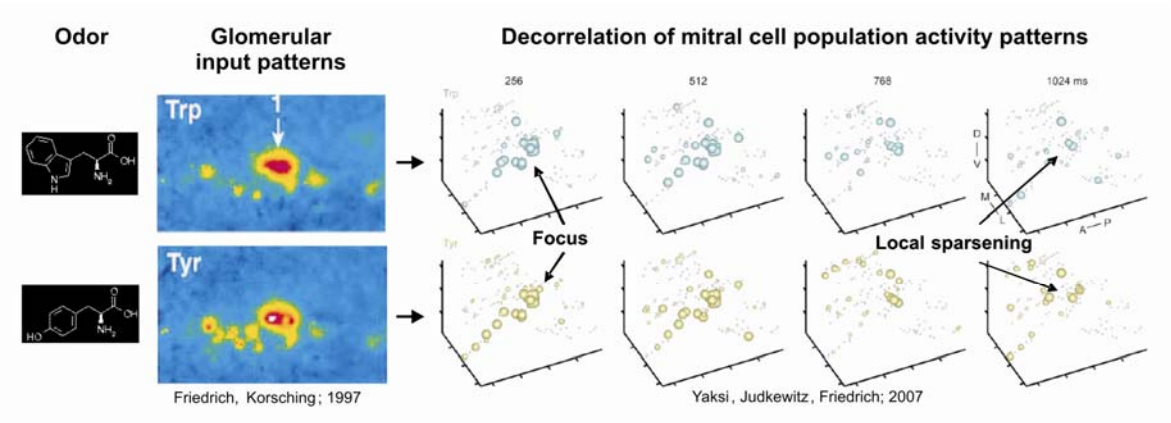

Figure 3 | Glomerular and mitral cell activity patterns evoked by the chemically similar odors tryptophan (Trp) and tyrosin (Tyr). The chemically similar odors tryptophane (Trp) and tyrosin (Tyr) evoke highly overlapping glomerular input patterns (left). This pattern overlap is also reflected in the initial mitral cell activity pattern (right, 3D reconstruction of MC activity patterns) which becomes decorrelated during the first 1000 ms.

double the number of responsive glomeruli (Friedrich and Korsching 1997; Meister and Bonhoeffer 2001; Wachowiak and Cohen 2001). Nonetheless, animals usually identify an odor as the same stimulus over a concentration range of two or three orders of magnitude (Krone, Mannel et al. 2001; Abraham, Spors et al. 2004; Uchida and Mainen 2007). This perceptual concentration-invariance is inconsistent with a processing strategy that generally decorrelates input patterns by amplifying small differences. It therefore remains unclear how the brain can perform pattern separation between similar molecules and – at the same time - pattern generalization across different odor concentrations.

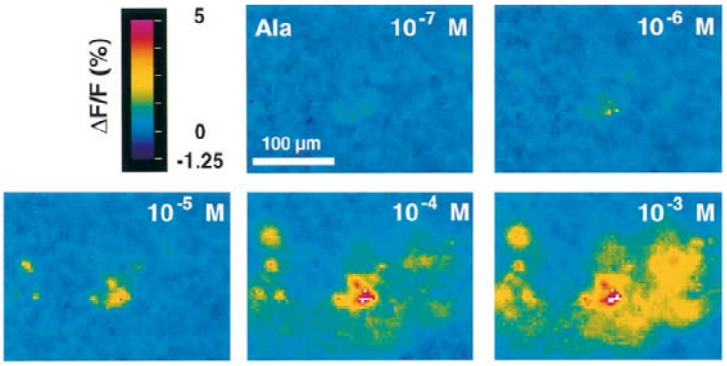

Figure 4 | Glomerular input patterns evoked by the odor alanin at 5 different concentrations (Friedrich, Korsching; 1997).

Attractor states as a potential pattern classificator in the OB neural network

These two contradictory computations – pattern separation and pattern generalization – cannot be achieved by a mechanism that simply transforms the input into a reflection of itself in the representation space (illustrated as a simplified 2-dimensional representation space in Fig. 5a). A possible solution to this problem is the classification of overlapping inputs into discrete output patterns such that some inputs converge onto a common output while others diverge onto separated outputs. This would require stable representation states in the network as illustrated by delimited local minima in a two-dimensional scheme of the state space (Fig. 5b, c; colored dots). Here, small input variations (e.g. evoked by different concentrations of the same odor, see also Fig. 4) would activate the same output activity pattern (Fig. 5b), while different stable states would be activated if the input variations exceed a particular threshold (Fig. 5c).

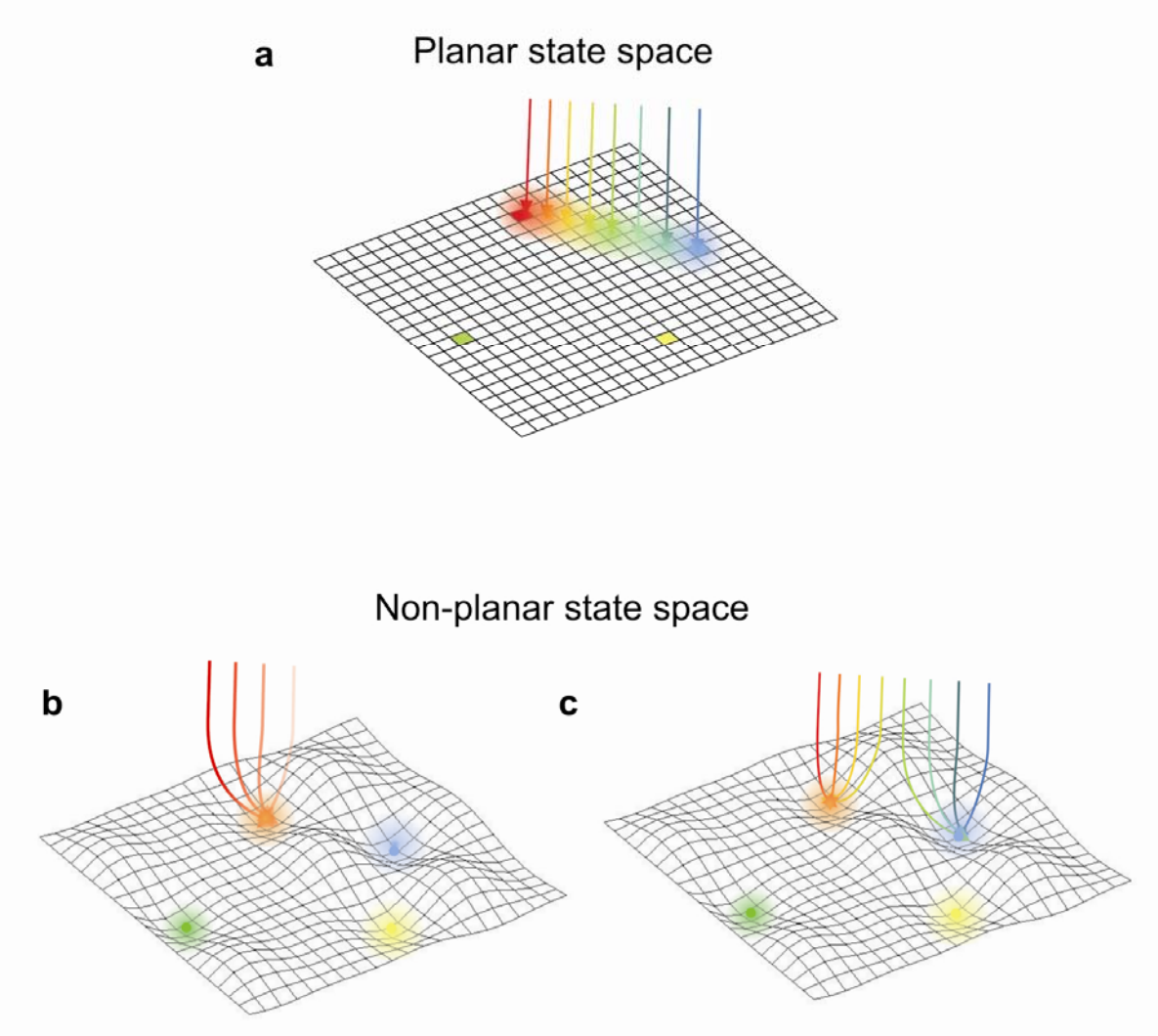

Figure 5 | Illustration of different forms of state spaces as two-dimensional landscapes. Different colors at the surface represent different stable representations (states). Arrows symbolize the input while different arrow colors denote differences in the input. **a**, Representations of continuously changing inputs in a planar state space. **b**, Convergence of slight input variations (e.g. different odor concentrations) on a discrete representation in a non-planar state space. **c**, Convergence of strong input variations (e.g. gradual transition between different odors) on a discrete representation in a non-planar state space (b and c: modified from scholarpedia)

Such a pattern classification mechanism can, in theory, be achieved by attractor networks (Hopfield 1982; Colgin, Moser et al. 2008; Wang 2008; Mozer 2009). In this class of networks, an input causes the system to move through the state space towards a defined and stable attractor state. These attractor states represent multiple discrete states in the neural network which become retrieved as soon as an input pattern activates a critical fraction of neurons related to the particular state. Since different representations become activated in a mutually exclusive fashion, overlapping input patterns have to compete for the retrieval of the different states. In this model overlapping input patterns evoked by identical stimuli would converge and thereby become invariant to input variations. Strong variations in the input – on the other hand - would cause the system to separate the overlapping input patterns into discrete output states. Such attractor networks have been proposed to mediate various neuronal computations including hippocampal remapping (Colgin, Moser et al. 2008), categorical face perception (Rotshtein, Henson et al. 2005), decision making (Machens, Romo et al. 2005) and sensory discrimination (Freeman and Grajski 1987). Nevertheless, only few studies have provided direct evidence that neuronal circuits can exhibit signatures of attractor dynamics (Taube 1995; Cossart, Aronov et al. 2003; Wills, Lever et al. 2005).

If neuronal circuits classify inputs into discrete outputs in an attractor-like fashion, gradual changes in the input should result in abrupt transitions between output patterns. This is a strong prediction that can be tested experimentally by gradually morphing of one stimulus into another. Such experiments have provided evidence for the discrete classification of spatial information by place cells in the hippocampus (Wills, Lever et al. 2005) (see also (Leutgeb, Leutgeb et al. 2005)). In the olfactory system, morphing of odors have been reported to result in a variety of different transitions in MC responses (Khan, Thattai et al. 2008). Hence, signatures of attractor dynamics are not obvious in responses of individual MCs, but a quantitative analysis of population activity patterns is necessary to directly address this question.

Aim of this study

To investigate whether olfactory input patterns are classified into discrete output states in the OB in an attractor-like fashion. One way to test this could be to stimulate the OB with varying but similar stimuli (e.g. varying concentrations of identical odors or background odors) and with a stimulus gradually changing its identity (e.g. morphing of one odor into another). Attractor dynamics should then be reflected in a robust invariance of activity evoked by variations of similar stimuli and in abrupt switches between different output representations evoked by gradually changing input patterns.

I performed two sets of experiments. First I presented different concentrations of the same odor to induce variations in the OB input. Secondly, I gradually morphed two odors into each other to force the transition between different pattern generalizations. Responses were measured in the OB of zebrafish by temporally deconvolved Ca^{2+} imaging (TDCa imaging) using 2-photon microscopy (Denk, Strickler et al. 1990). This method detects action potential firing with high sensitivity and reconstructs spatio-temporal patterns of firing rate changes across large populations of neurons (Yaksi and Friedrich 2006). MC activity patterns evoked by the same odor remained correlated within a substantial concentration range, consistent with concentration-invariant odor recognition (Krone, Mannel et al. 2001; Abraham, Spors et al. 2004). Morphing of odors, however, resulted in abrupt pattern transitions that were mediated by relatively small ensembles of MCs. The OB therefore classifies inputs into discrete output patterns and thereby creates partially concentration-invariant, noise-resistant odor representations. This pattern classification is consistent with attractor dynamics and perceptual phenomena such as odor masking and the configural perception of odor mixtures.

Material and Methods

Animals, dye loading and odor stimulation.

All animal procedures were performed in accordance with official animal care guidelines and approved the Veterinary Department of the Canton of Basel-Stadt (Switzerland). Experiments were performed in 38 adult zebrafish (Danio rerio; > 3 month old). Measurements of MC activity patterns were performed in a transgenic line (HuC-YC) that expresses the yellow-flourescent marker protein, yellow cameleon 2.1 (YC) (Miyawaki, Llopis et al. 1997; Higashijima, Masino et al. 2003), selectively in MCs in the OB (Fig. 8a) (Li, Mack et al. 2005). For anaesthesia fish were put on ice in ringer solution (table 1) to avoid local differences in osmolarity during the following dissection by remaining water. As soon as the animal stopped moving it was decapitated. Then the eyes, jaws and bones were removed over the ventral telencephalon to expose the OBs. Finally the dura of the OBs were carefully removed by a blunt forcept. The whole dissection was performed in pre-oxygenized ringer solution on ice. The resulting explant preparation of the intact brain and nose was then superfused continuously with an oxygenized ringer solution (table 1). This solution was similar to teleost artificial cerebrospinal fluid but contained HEPES instead of carbonate for pH buffering (Mathieson and Maler 1988).

Chemical component	**Molarity**
NaCl	124 mM
Glucose	10 mM
KCl	2 mM
MgSO4	1.6 mM
CaCl	2 mM
KH2PO4	1.25 mM
NaHCO3	24 mM
HEPES	25 mM
NaGluconate	15 mM
NaOH	9 mM

Table 1 | Components of ringer solution for adult zebrafish.

The preparation was warmed up to room temperature. 50 µg of the Rhod2-AM calcium dye were dissolved in 16 µl DMSO/Pluronic Acid F-127 (80/20). For each experiment 3 µl of the dye were diluted 1:10 in oxygenized ringer solution and 5 µl of the dye were loaded into a glass injection pipette. The ventrolateral region of the OB was located under control of the transmission optics of the microscope. Injection was performed at ~3 locations per plane and repeated in 4-5 planes until a uniform staining of the lateral OB was achieved. The distance between each injection was approximately 30 µm. Measurements started 30 – 60 min after termination of the dye loading procedure. Odors were of the highest available purity (≥99.0% (NT), Fluka, Neu-Ulm, Germany) and applied through a constant flow directed at the ipsilateral naris using a computer-controlled, pneumatically actuated HPLC injection valve (Rheodyne) (Fig. 6). The rise time of the stimulus was approximately 600 ms, followed by a plateau of approximately two seconds and a slow decay. Stimuli were delivered in a pseudo-random sequence to minimize hysteresis effects and separated by at least 90 seconds to avoid sensory adaptation. Each odor stimulus was repeated twice and responses were averaged.

Temporally deconvolved calcium imaging of MC activity.

Most imaging experiments were performed in the ventro-lateral OB that contains most of the amino acid-responsive MCs (Yaksi, von Saint Paul et al. 2009). Only responses depicted in Fig. 12 have also been measured in the ventro-medial region of the OB. In different fish, MC responses were therefore measured from the same region but not necessarily from MCs connected to equivalent glomeruli. Within a given focal plane raw calcium signals from genetically identified MCs were initially measured in response to the odor at 10^{-5} M (concentration experiments), or to the 50/50 mixture or the pure odors (morphing experiments). If none of the MCs responded to these odors, a new focal plane was selected. If a focal plane clearly contained responsive MCs, responses of all MCs in this plane were included in the data set.

This procedure reduces the number of non-responsive MCs in the data set but should have only minimal consequences on the results because non-responsive neurons do not change the general outcome of the multivariate analyses. In each

fish, MCs from 3 – 4 focal planes were measured usually (Fig. 6). Odor-evoked calcium signals were measured using a custom-built two-photon fluorescence microscope equipped with a mode-locked Ti:Sapphire laser (SpectraPhysics) and a 20 x Objective (NA 1.0, Zeiss). Yellow (YC) and red (rhod-2) fluorescence emission was detected externally by a photomultiplier based whole-field detector through emission filters (515/30 and 610/75 nm). Laser intensity was adjusted in each focal plane to minimize photobleaching. Each individual recording lasted 12.8 seconds and was performed at a frame rate of 8 Hz (mixture experiments, 100 frames, 128x128 pixels, 1ms/line) or 4 Hz (concentration experiments, 50 frames, 256x256 pixels, 1ms/line) and was performed by SCANIMAGE software (http://svobodalab.cshl.edu/) (Pologruto, Sabatini et al. 2003).

Series of fluorescence images were averaged across trial repetitions and converted into image series depicting the relative change in fluorescence (ΔF/F)

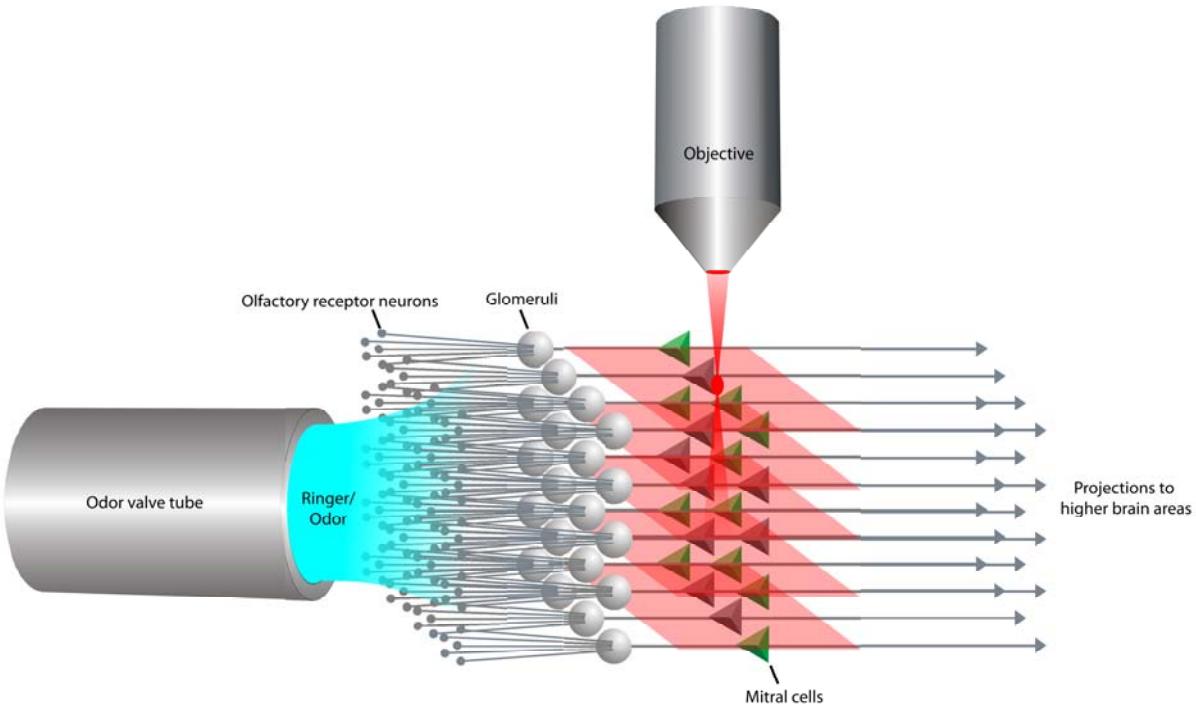

Figure 6 | Illustration of the imaging procedure during odor stimulation

in each pixel (Fig. 7b). The baseline fluorescence F was calculated by averaging the raw pixel values over at least one second before onset of the odor stimulus. Time-averaged maps of calcium signals were calculated by averaging the ΔF/F images over a period of approximately three seconds after activity onset. MC somata were identified in images of YC fluorescence and outlined manually (Fig.

7a, b). Firing rate changes were reconstructed from the time course of the calcium signal in each MC by temporal deconvolution as described (Fig. 7 c, d) (Yaksi and Friedrich 2006). Parameters used for deconvolution were τ_{decay} = 3 s and thr_{noise}= 1%. TDCa signals were then low pass filtered again using a 1-pole Butterworth filter with a cutoff frequency of 0.2 times the frame rate in both directions. This additional filtering step further increases the accuracy of firing rate reconstructions in each time bin, as found by a direct comparison between TDCa signals and simultaneously measured action potentials (Yaksi and Friedrich 2006). However, it also slightly broadens the time course of TDCa signals, which accounts for the apparent increase of the TDCa signal before stimulus onset in some cases.

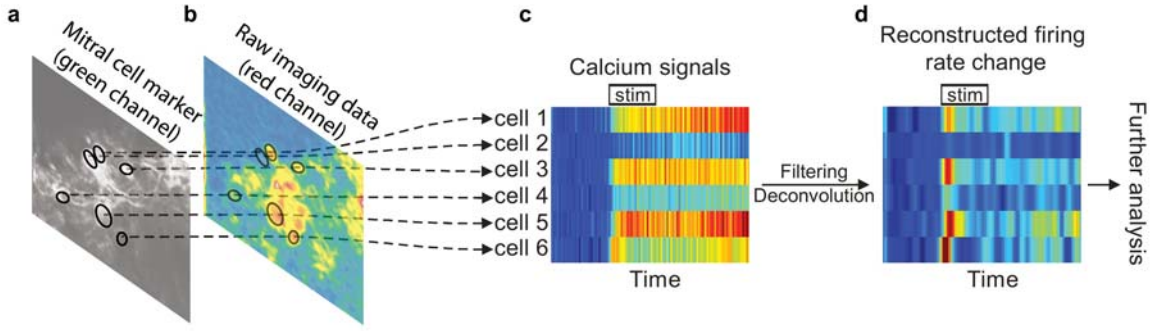

Figure 7 | Simplified scheme of the basic data analysis procedure. a, Example for an image for mitral cell selection expressing YC under the HUC-promotor. **b**, Time-averaged image of relative change in fluorescence (ΔF/F) with 6 somata selected corresponding to MCs in (a). **c**, Raw calcium signal time-course of MCs selected in (a) and (b). **d**, Reconstructed firing rate changes after filtering and deconvolution of the raw calcium signals in (c).

Calcium imaging of glomerular activation patterns.

Calcium signals from afferent axon terminals were measured after loading of Oregon Green 488 BAPTA-1-dextran (OGB1-dextran; 10 kD; Invitrogen) into olfactory sensory neurons as described (Friedrich and Korsching 1997). For this procedure the zebrafish was initially anesthetized in 0.01 % tricaine methanesulfonate (MS-222) and fixated under a binocular scope by wrapping the fish into a wet paper towel. To maintain anesthesia and vital functions a tube was placed into the mouth of the fish and the gills were superfused continuously by a slow flow of fishtank-water with 0.01 % tricaine methanesulfonate (MS-222). A

solution of 2 – 5 % OGB1-dextran was then infused into the noses for five minutes. After 3 – 6 days, odor-evoked calcium signals were measured in the ventrolateral region of the OB in the explant preparation. Measurements have been done by means of epifluorescence optics (objective: 20 x; NA, 1.0; Zeiss) and a sensitive CCD camera (CoolSnap; Photometrics) acquiring 100 frames (12.8 seconds) with an exposure time of 128 ms/frame (pixel binning = 4 x 4).

Data Analysis

Data analysis was performed using routines written in IgorPro (Wavemetrics) and MATLAB (The Mathworks, Natick, MA). For some analyses, data acquired at 128 ms/frame were down-sampled to 256 ms/frame by averaging successive frames. Before the second low-pass filtering step, TDCa signals were normalized to the maximum of the average MC responses in each experiment. TDCa signals measured in different experiments were then aligned in time on the onset of the population response in each experiment. After temporal alignment, data from different experiments were pooled. Time t = 0 was assigned to the onset of the mean activity in the pooled data set by defining the time when the mean activity clearly deviates from the baseline. Because it is sometimes difficult to unambiguously define this time point I tested different methods (manual detection, different fixed thresholds, different thresholds based on the s.d.) and found that the time defined as t = 0 varied maximally by 256 ms, usually less. Pooled response matrices were then low-pass filtered (see above), which smeared out the TDCa signals in time over a period of at least 384 ms. Hence, the potential imprecision in determining t = 0 is relatively small compared to the effect of low-pass filtering. The broadening of TDCa signals by lowpass filtering should be considered in the interpretation of response time courses. MCs were counted as responsive in a given time bin when the TDCa signal exceeded two times the s.d. of the baseline corrected TDCa signal from the same cell in the absence of odor stimulation. The s.d. was calculated from 10-second measurements without odor stimulation in separate trials.

To compute trajectories in principal component space, matrices containing cells as rows and stimuli as columns at each time bin were appended columnwise,

resulting in one matrix containing all cells as rows and all stimuli in each time bin as columns (number of colums = stimuli x time bins). Principal components were then extracted after standardizing columns to obtain one coefficient (loading) for each stimulus and time bin on each principal component. Principal components are orthogonal basis vectors representing the variance in the original data set in decreasing order. The coefficients of each odor on the first three principal components therefore visualize odor-evoked activity patterns in an orthogonal 3-D space that retains the maximum possible variance in the data. For plots of trajectories, data points were interpolated between time bins. Principal component analysis on patterns in the steady state was performed using the same procedure on time-averaged activity patterns (number of time bins = 1).

To confirm the robustness of results from correlation and principal component analysis, I created reduced data sets by randomly selecting 50% of the MCs and reapplied multivariate analyses on these data sets. This procedure was repeated at least 10 times for each data set. As shown in Fig. 23, similar results were obtained in different subsets, demonstrating that results were not biased by small sampling size. Moreover, similar results were usually obtained when data were analyzed from individual animals (Fig. 16b; Fig. 21b). Correlations between patterns of spontaneous calcium signals or between shuffled activity patterns were near zero (Fig. 16c, d).

Calcium signals measured in glomerular afferents after loading of OGB1- dextran were not temporally deconvolved. In rodents, transmitter release from axons of olfactory sensory neurons depends almost linearly on the intracellular calcium concentration and raw calcium signals are highly correlated to transmitter release (Bozza, McGann et al. 2004; Murphy, Glickfeld et al. 2004). The time course of the raw calcium signal is therefore likely to be a good estimator for transmitter release and, thus, synaptic input to OB neurons. Nevertheless, I also determined the time constant of calcium transients in axon terminals of sensory neurons by measuring calcium transients in response to electrical stimulation of the olfactory nerve. I found that the time constant to be very short compared to the time constant of calcium transients in MC somata (~100 ms). Deconvolving calcium signals from glomerular afferents with this time constant changed the time course

of signals only minimally. As a consequence, the effect on correlations was negligible.

To sort transitions between mitral cell responses into different categories (Fig. 26), responses of each MC to series of different concentrations or mixture ratios were fit by linear, quadratic and sigmoid functions (Leutgeb, Leutgeb et al. 2005; Khan, Thattai et al. 2008). For each fit, the variance explained by the fit relative to the non-explained variance (F statistic) was calculated, which takes into account the different degrees of freedom for the different functions. To calculate the variance, the mean was not subtracted in order to include responses that are significant but constant over the stimulus series. Input parameters for linear and quadratic fitting functions do not take any effect on the quality of the fit and have therefore been kept constant during the analysis. In contrast 8 different input parameter variations have been tested for each sigmoid fit of MC responses (4 different x-offset parameters x 2 different slopes) in order to maximize the fitting quality. The 8 different fitting parameters have been determined manually and where optimized for the respective type of experiment (mixture- or concentration experiment). The sigmoid fit which explained most of the variance (highest F-value) was selected for further analysis. MCs that did not show a response that was fit statistically significant ($P > 0.05$) were excluded from further analysis. Each response was then assigned to the function fit category (linear, quadratic or sigmoid) that explained the highest fraction of the variance (highest F-statistic). Statistical comparisons were performed using a non-parametric Mann-Whitney U-test. All correlation values are Pearson product moment correlations.

Results

In order to measure odor-evoked changes in firing rates across large numbers of MCs I loaded OB neurons in an explant preparation of the intact brain and nose (Tabor, Yaksi et al. 2004) with the red-fluorescent Ca^{2+} indicator, rhod-2-AM, by bolus injection (n = 38 fish) (Brustein, Marandi et al. 2003; Stosiek, Garaschuk et al. 2003; Yaksi and Friedrich 2006). Odor-evoked changes in rhod-2 fluorescence were measured in the amino acid-sensitive ventrolateral part of the OB by two-photon microscopy (Denk, Strickler et al. 1990). MCs were identified by simultaneous imaging of a yellow-fluorescent marker protein expressed under the control of a MC-specific promoter (HuC-YC; (Higashijima, Masino et al. 2003; Li, Mack et al. 2005)). Firing rate changes of each neuron were then reconstructed by temporal deconvolution of Ca^{2+} signals with a kernel representing a Ca^{2+} transient evoked by a single action potential (Yaksi and Friedrich 2006). This method detects action potential firing with high sensitivity and reconstructs spatio-temporal patterns of firing rate changes across large populations of neurons (Yaksi and Friedrich 2006).

Responses of individual MCs to different odor concentrations

In order to identify concentration-invariant components in MC activity patterns I first measured responses of MCs to the amino acid lysine (Lys; n = 140 MCs from 4 OBs) and phenylalanine (Phe; n = 128 MCs from 7 OBs) at five different concentrations (10^{-3} M, 10^{-4} M, 10^{-5} M, 10^{-6} M and 10^{-7} M). Amino acids are natural odors for zebrafish with response thresholds in the nanomolar range and maximal concentrations within food sources in the millimolar range (Carr 1988; Michel and Lubomudrov 1995). The concentration series is therefore assumed to cover most of the physiological range. In addition, the stimulus panel contained a blank and a chemically related control odor (arginine [Arg] for concentration series of Lys; tryptophan [Trp] for concentration series of Phe) at 10^{-5} M. Previous studies demonstrated that MC activity patterns evoked by the control odor and the test odor are initially similar but subsequently become decorrelated during the dynamic phase of the odor response (Friedrich and Laurent 2001;

Friedrich, Habermann et al. 2004; Friedrich and Laurent 2004; Yaksi, Judkewitz et al. 2007). Hence, higher brain areas receive discretized input from the OB (Yaksi, von Saint Paul et al. 2009).

Responses of MCs were dynamic and concentration-dependent (Fig. 8a, b; Fig. 9 a, b). In general, higher odor concentrations decreased response latency and recruited more MCs, resulting in a larger mean response to Lys (Fig. 8a-c) but not to Phe (Fig. 9c). Concentration-response functions of individual MCs were, however, diverse (Fig. 8b, Fig. 9b, Fig. 26). Response amplitudes of some MCs increased with concentration whereas others were maximal at intermediate or low concentrations (Fig. 8b; Fig. 9b). Moreover, response amplitudes and time courses of some MCs changed gradually with concentration (Fig. 8b, MC 1, 2, 3; Fig. 9b, MC 2, 3, 4) while others changed more abruptly (Fig. 8b, MC 4, 5; Fig. 9b, MC 1, 5; Fig. 26).

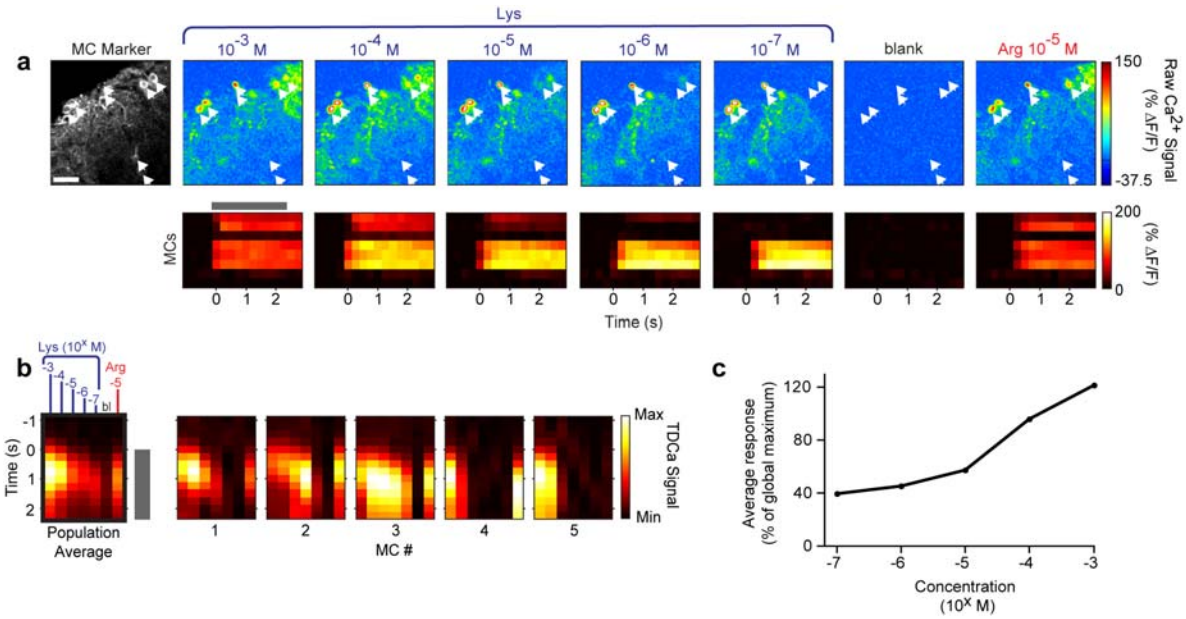

Figure 8 | Concentration-dependence of mitral cell activity patterns. **a**, Image of MC marker (left) and time-averaged raw calcium signals evoked by different concentrations of Lys, a blank, and the similar control odor Arg. Bottom: Raw calcium signals of MCs depicted by arrows as a function of time (gray bar indicates stimulation period). Scale bar: 25 µm. **b**, Left: Temporally deconvolved calcium signals (TDCa signals) evoked by the same stimuli averaged across the population of recorded MCs (n = 140 MCs from 4 OBs) as a function of time. Right: Five examples of single MC responses to the set of stimuli. Gray bar indicates odor stimulation. **c**, Mean population TDCa signal averaged over time (0 – 1920 ms) as a function of increasing concentration.

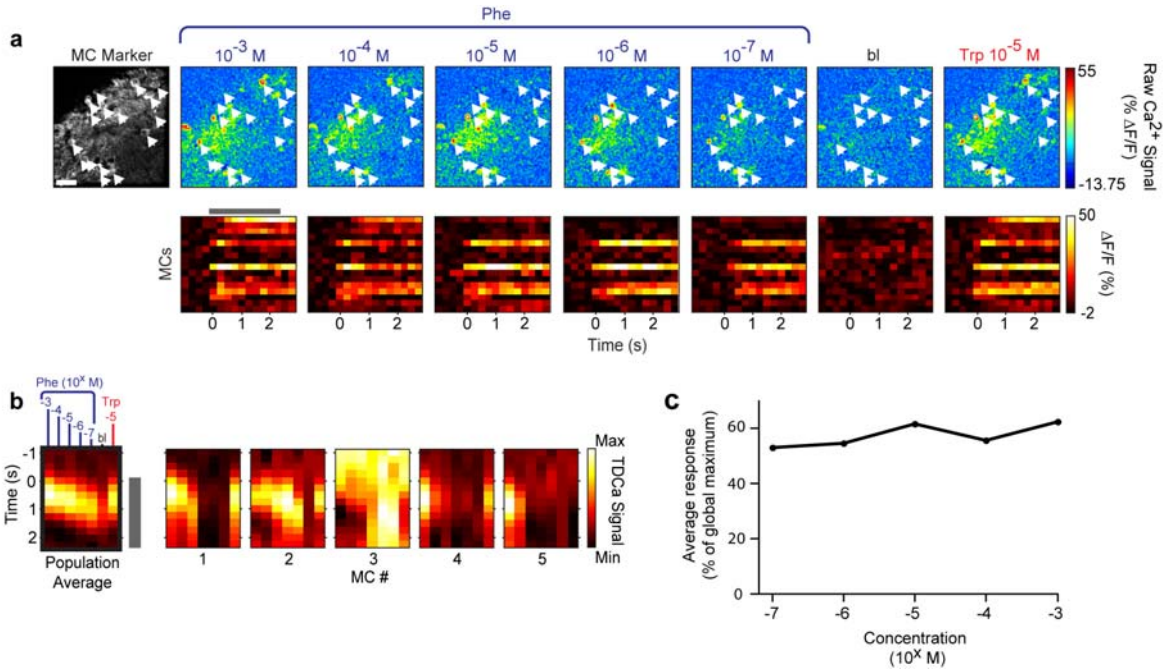

Figure 9 | Concentration-dependence of mitral cell activity patterns. **Second odor example** **a**, Image of MC marker (left) and time-averaged raw calcium signals evoked by different concentrations of Phe, a blank, and the similar control odor Trp. Bottom: Raw calcium signals of MCs depicted by arrows as a function of time (gray bar indicates stimulation period). Scale bar: 25 µm. **b**, Left: Temporally deconvolved calcium signals (TDCa signals) evoked by the same stimuli averaged across the population of recorded MCs (n = 128 MCs from 7 OBs) as a function of time. Right: Five examples of single MCs to the set of stimuli. Gray bar indicates odor stimulation. **c**, Concentration-response functions of averaged TDCa signals.

Concentration-dependence of population activity patterns

The diversity of single cell response functions to odor concentration changes makes it difficult to derive a consistent explanation for perceptual concentration invariance as well as for concentration-dependent odor quality changes. It further implies that odor-encoding activity patterns across the population of MCs change with odor concentration in a complex fashion. I therefore analyzed MC responses as patterns by combining responses of all MCs to all stimuli into response matrices, one for each time bin. The response of the MC population to a given stimulus in a given time window was thus represented by a vector. In order to determine the similarity between different activity patterns at different

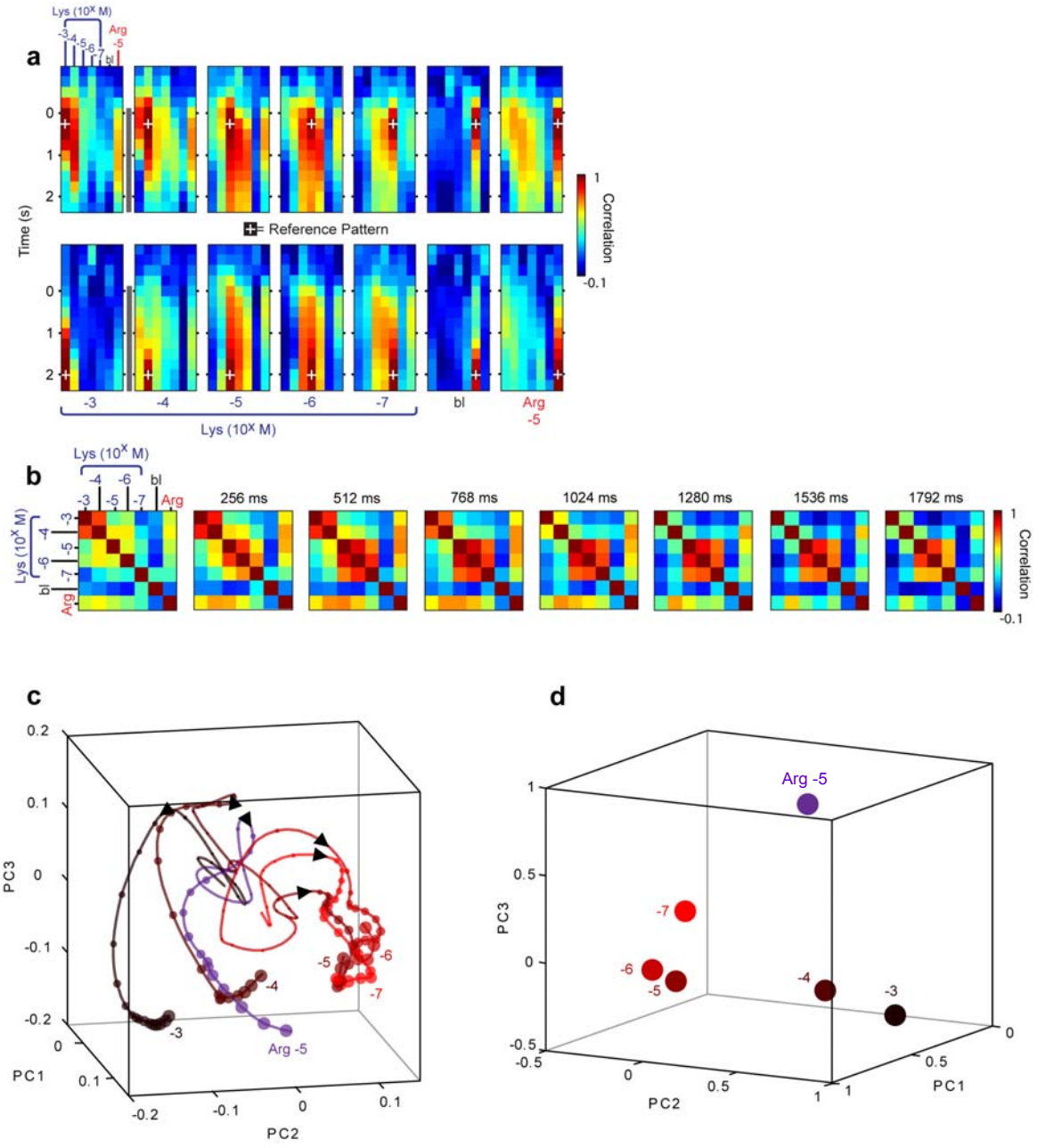

Figure 10 | Population activity patterns at different odor concentrations of Lys. a, Correlation analysis of activity patterns evoked by different concentrations of Lys, a blank, and Arg at 10^{-5} M at different time points during the response (n = 140 MCs from 4 OBs). Each panel depicts the correlation coefficients between a reference pattern (indicated by a white cross) and the activity patterns evoked at all time bins under stimulation with all different stimuli. Top row shows correlations between evoked activity and reference patterns selected from an early response time (256 ms after response onset). Reference patterns in bottom row were selected from a later time point during the response (2048 ms). **b**, Analysis showing the correlations between activity patterns evoked by all different stimuli in individual time slices **c**, Trajectories of odor-evoked activity patterns (-2048 ms - 4096 ms) in the space spanned by the first 3 principal components. Increasing plot symbols indicate the direction of time (interval between symbols: 256 ms) and arrowheads represent the onset of the odor response. **d**, Time-averaged (1536 – 2304 ms) MC activity patterns in principal component space.

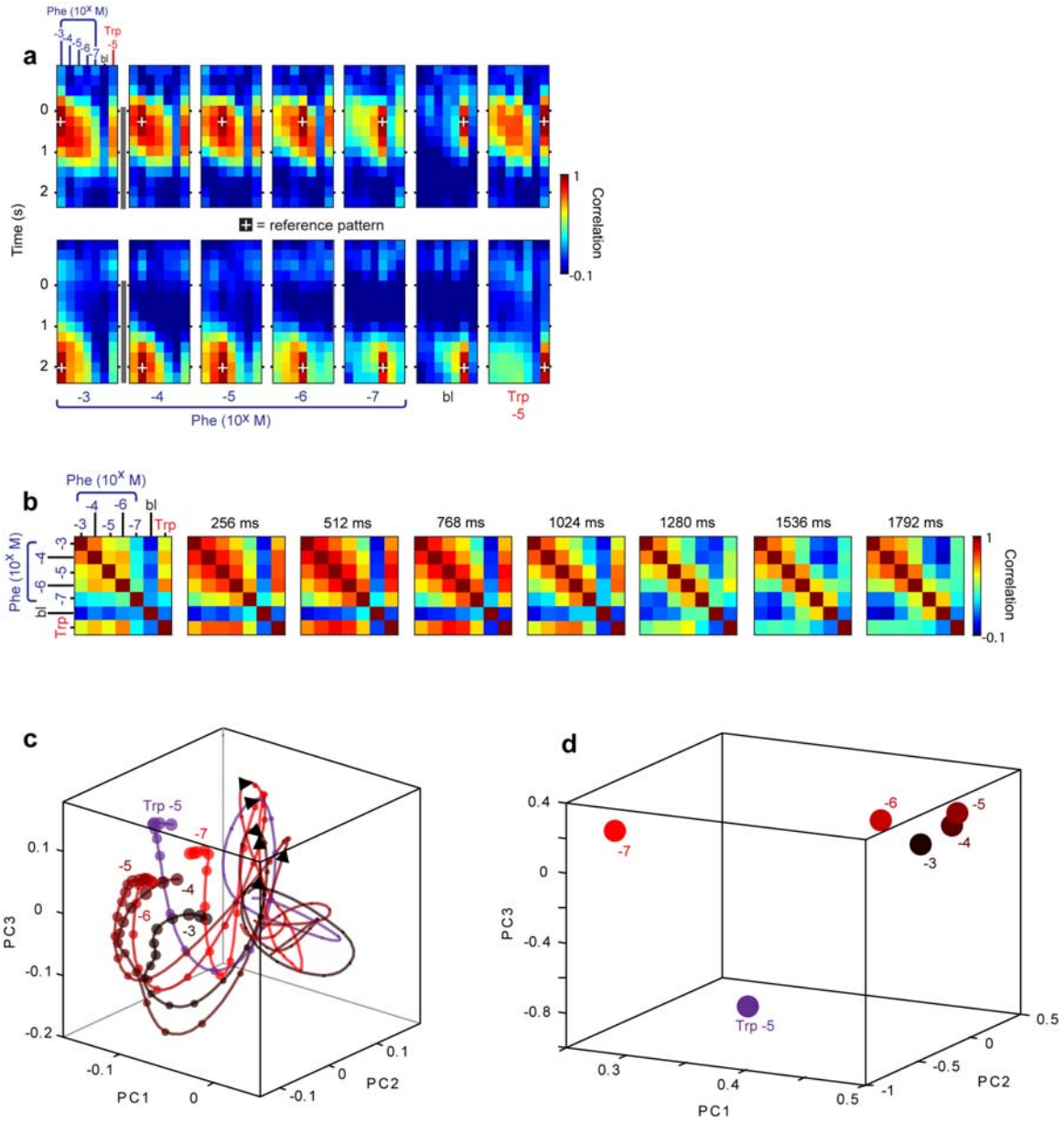

Figure 11 | Population activity patterns at different odor concentrations of Phe. a, Correlation analysis of activity patterns evoked by different concentrations of Phe, a blank, and Trp at 10^{-5} M at different time points during the response (n = 128 MCs from 7 OBs). Each panel depicts the correlation coefficients between a reference pattern (indicated by a white cross) and the activity patterns evoked at all time bins under stimulation with all different stimuli. Top row shows correlations between evoked activity and reference patterns selected from an early response time (256 ms after response onset). Reference patterns in bottom row were selected from a later time point during the response (2048 ms). **b**, Correlation analysis showing the correlations between activity patterns evoked by all different stimuli in individual time slices **c**, Trajectories of odor-evoked activity patterns (-2048 ms - 4096 ms) in the space spanned by the first 3 principal components. Increasing plot symbols indicate the direction of time (interval between symbols: 256 ms). Arrowheads represent the onset of the odor response. **d**, Time-averaged (1536 – 2304 ms) MC activity patterns in principal component space.

times, I selected two reference patterns (vectors) for each stimulus, one at an early time point (256 ms after response onset) and one at a late time point (2048 ms). The similarity between each reference pattern and patterns evoked by all stimuli at all times was then quantified by the Pearson correlation coefficient of the corresponding vectors (Fig. 10a; Fig. 11a). In addition, I calculated time series of correlation matrices that represent the pairwise correlations between all activity patterns within each time bin (Fig. 10b; Fig. 11b).

The mean correlation between activity patterns evoked by Lys (10^{-7} M – 10^{-5} M) and the structurally similar control odor Arg (10^{-5} M) was 0.58 ± 0.11 early during the odor response (256 – 512 ms; Fig. 10a, b) and significantly lower at a late response time (0.30 ± 0.08; $P < 0.001$, regression analysis; 2048 – 2304 ms). A similar decrease in correlation was observed for activity patterns evoked by Phe between 10^{-6} M – 10^{-3} M and the control odor Trp at 10^{-5} M (0.77 ± 0.07 at early response time; 0.42 ± 0.04 at late response time; Fig. 11a, b). Hence, activity patterns evoked by structurally similar odors were decorrelated during the later odor response, consistent with previous results (Friedrich and Laurent 2001; Friedrich, Habermann et al. 2004; Friedrich and Laurent 2004; Yaksi, Judkewitz et al. 2007). Moreover, early reference patterns were often only weakly correlated with activity patterns evoked by the same odor at later response times and vice versa (Fig. 10a; Fig. 11a), indicating that odor-evoked activity patterns become reorganized during the initial phase of an odor response (Friedrich and Laurent 2001; Friedrich, Habermann et al. 2004; Friedrich and Laurent 2004; Yaksi, Judkewitz et al. 2007).

Early during the odor response, activity patterns evoked by different concentrations of the same odor were highly correlated within a concentration range of approximately two to three orders of magnitude (10^{-7} M – 10^{-5} M for Lys; 10^{-6} – 10^{-3} M for Phe; Fig. 10a, b; Fig. 11a, b). Surprisingly, these high correlations were maintained at later time points, despite the reorganization of activity patterns. The mean correlation between activity patterns evoked by Lys at concentrations between 10^{-7} M and 10^{-5} M was 0.76 ± 0.10 (Mean ± SD; quantified from Fig. 10b) early during the odor response (256 – 512 ms) and not significantly different in a late time window (0.67 ± 0.09; $P > 0.05$, regression analysis; 2048 - 2304 ms). Likewise, correlations between activity patterns

evoked by Phe between 10^{-6} and 10^{-3} M did not decrease substantially between the early (0.77 ± 0.09) and the late (0.65 ± 0.10) reference time (Fig. 11b). Hence, activity patterns evoked by different concentrations of the same odor are reorganized, but not decorrelated during the initial phase of the odor response.

To confirm this result I visualized the dynamics of odor-evoked activity patterns using principal component analysis. This technique reduces the dimensionality of activity patterns from n (number of MCs) to three while retaining the maximum possible amount of variance. In the orthogonal coordinate system defined by the first three principal components, instantaneous activity patterns are therefore represented by points and time series of activity patterns are represented by trajectories.

Each trajectory moved from a resting state (spontaneous activity) to a defined subspace representing the steady-state response pattern after the initial reorganization. Trajectories evoked by Lys at 10^{-4} M and 10^{-3} M and by Arg (10^{-5} M) projected to different subvolumes (Fig. 10c), indicating that activity patterns become separated. Trajectories evoked by 10^{-7} M – 10^{-5} M Lys, in contrast, projected to overlapping subvolumes (Fig. 10c), consistent with their high correlation (Fig. 10a, b). To further optimize the visualization of activity patterns after the dynamic phase of the odor response, I time-averaged activity patterns between 1536 ms – 2304 ms (steady state) after response onset and plotted them in principal component space (Fig. 10d). As observed before, steady-state responses patterns evoked by 10^{-7} M – 10^{-5} M Lys were clustered and separated from responses to lower concentrations or control odor. Different concentrations of Phe also produced trajectories that remained clustered within a certain concentration range (10^{-6} M – 10^{-3} M) but diverged from trajectories representing lower concentrations (10^{-7} M) or a different odor (Trp, 10^{-5} M; Fig. 11c). Likewise, PCA analysis of averaged steady-state activity patterns reveals a tight clustering of responses to Phe at concentrations between 10^{-6} M – 10^{-3} M while responses to lower concentrations or the control odors are separated (Fig. 11d).

Taken together, the OB separates activity patterns evoked by molecularly different odors but preserves the similarity of odor representations across concentrations.

Representation of binary odor mixtures

I found that input from molecularly different odors becomes decorrelated while strong correlations between inputs from similar odors are retained. This finding suggests a mechanism that generates stable network states which are very tolerant to input variations. Such a mechanism would require sharp transitions between different states in order to minimize overlapping activity patterns in the transition phase. If this hypothesis is true the response amplitude and firing pattern evoked in a single MC by a binary equimolar odor mixture should not reflect the sum of the responses to the two odor components but should rather correspond to only one of the components in accordance with either one or the other side of the transition. To test this hypothesis I imaged MC responses in the OB to individual odors and binary mixtures of the amino acids arginin, tyrosin, tryptophan and the bile acid TDCA (Arg, Tyr, Trp, BA and the binary mixtures Arg/Tyr, Trp/Tyr, BA/Tyr and BA/Arg). While BA is chemically very different from all amino acid odors, Trp and Tyr share the same secondary molecular features (aromatic side chain). These odors give therefore rise to highly similar glomerular input patterns, while input patterns evoked by Arg strongly differ from those evoked by Tyr and Trp (Friedrich and Korsching 1997). Signals were detected by a detection threshold that was determined by multiplying the standard deviation of the Ca^{2+} signal in trials without odor stimulation with the factor 2. To avoid artifacts from signals which are close to this threshold, neuron-mixture pairs were included in the analysis only when at least one response exceeded the detection threshold three times. This analysis revealed that all MCs responding to a mixture also responded to at least one component (n = 59 MC-odor pairs from 4 fish; Fig. 12a, b). In turn, 96% of MCs which responded to a component also responded to the mixture involving this component. To test the hypothesis that mixture response amplitudes reflect the amplitude of only one component, responses were rescaled so that the smaller component equals 0 and the larger component equals 1 (Fig. 12b, middle). Mixture responses mapped onto this scale reveal that in most cases their amplitude equals 0 or 1. Hence, responses to odor mixtures indeed reflect the response amplitude evoked by only one of the components rather than a sum or average of both components. Earlier observations made in electrophysiological recordings of MCs in the zebrafish OB showed that slow temporal firing patterns evoked in

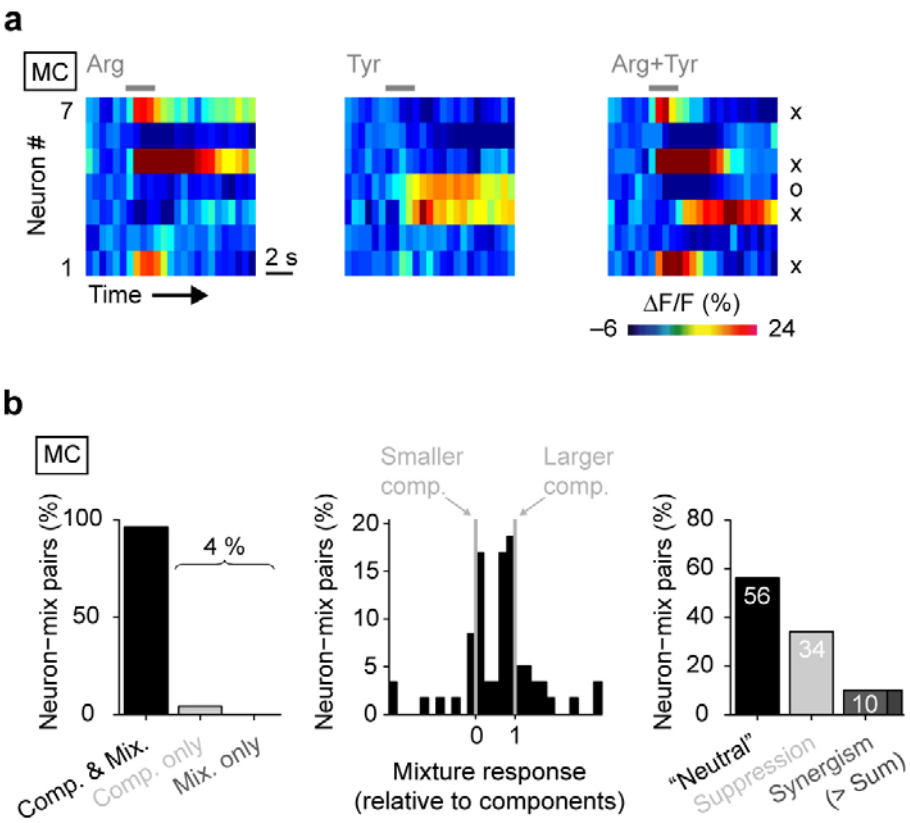

Figure 12 | Single neurons mixture interactions in the OB. **a**, Responses of 7 MCs to two individual odors and their binary mixture. Neurons in each panel were imaged at the same time. 'x' and 'o' indicate whether the stronger or weaker component response dominated the mixture response, respectively. **b**, Left, Neuron-mixture pairs (%) that showed clear responses to the binary mixture and a component (Comp. & Mix.), only to the components (Comp. only) or only to the mixture (Mix. only). Middle, histogram of mixture response strength compared to the component responses. Response magnitudes of the smaller component response was defined as 0 and the larger component response was set to 1. Mixture responses were scaled into this metric. Right, Percentage of neutral mixture responses, mixture suppression and mixture synergism. n = 59 neuron-mixture pairs.

individual MCs by equimolar odor mixtures usually also correspond to the pattern evoked by only one odor component (Tabor, Yaksi et al. 2004).

In the next step interactions between mixture evoked responses were further investigated by analyzing mixture synergism and mixture suppression (Fig. 12b, right). Mixture synergism was defined as a mixture evoked response that exceeds the response to the larger component, multiplied by a safety factor CV_{rep} to minimize false positives caused by the natural response variability. The safety

factor was defined as 1 + CV_{rep} which is the mean coefficient of variations of responses evoked by repeated applications of the same odor. Accordingly, suppression was defined as a response that was smaller than the larger component multiplied by the safety factor defined as 1-CV_{rep}. This analysis revealed that most MC-mixture pairs showed no synergism or suppression (56%). However, while synergism was rare (10%), suppression was observed in 34% of the MC-mixture pairs. Taken together, this analysis shows that single MC responses to odor mixtures usually correspond to one dominant component response but not the other. Moreover, mixture interactions, such as suppression or synergism, was observed only for a small fraction of MC-mixture pairs.

Abrupt transitions between representations during odor morphing in MC populations

MC responses in the OB evoked by equimolar binary odor mixtures were found to correspond to one of the components in both, amplitude and temporal patterning (Tabor, Yaksi et al. 2004). Summation of responses in amplitude or firing rate modulation has only been observed rarely. These findings suggest a mechanism that classifies the odor responses in either one or the other category with a sharp transition between them. To further investigate the transition between odor representations at a higher resolution I morphed one odor into another through a series of intermediate mixtures (100/0, 99/1, 90/10, 70/30, 50/50, 30/70, 10/90, 1/99, 0/100). I first tested whether an abrupt transition can already be found in the input of the MCs. To this end I recorded glomerular signals evoked by this set of stimuli. This was done by imaging calcium responses of the axon terminals of the olfactory receptor neurons (ORNs) within the glomeruli of the OB after loading of the ORNs with the calcium sensitive dye Oregon Green 488 BAPTA-1-dextran (Friedrich and Korsching 1997). For morphing experiments I first tested two structurally similar odors, Phe (10^{-5} M) and Trp (10^{-5} M). Responses from individual glomeruli share a stereotypic time course and have an average rise time of ~500 ms. (n = 118 glomeruli in 5 fish, Fig. 13a). Glomerular input activity patterns appear not to change much during morphing of Phe into the similar odor Trp. This is also confirmed by correlation analysis of glomerular activation patterns evoked by different mixture ratios of

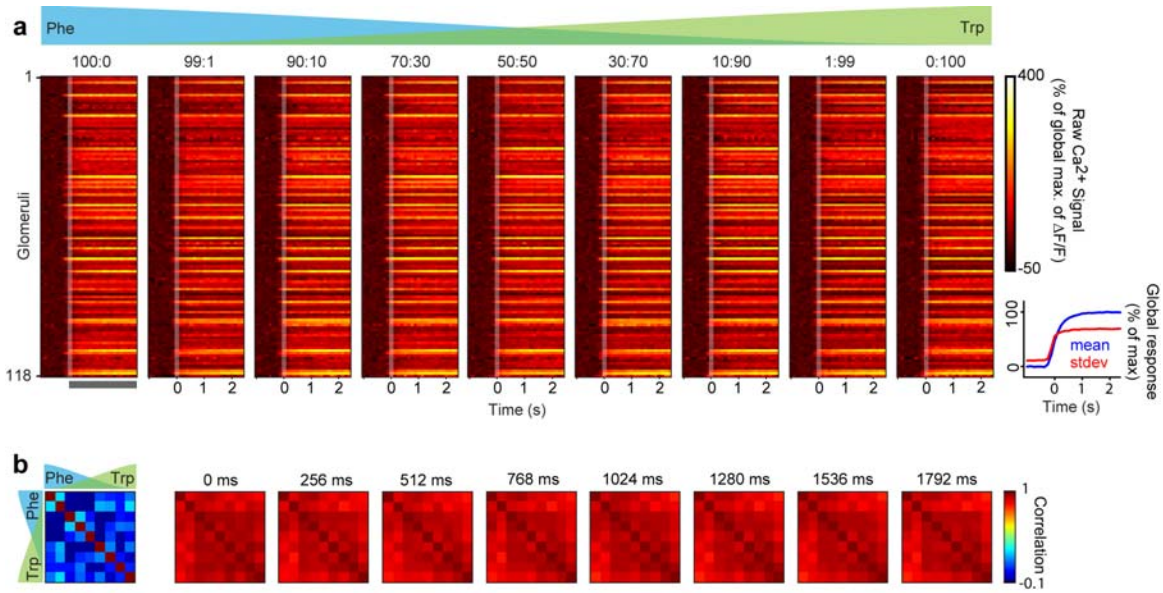

Figure 13 | Glomerular activation patterns in the OB during morphing of similar odors. a, Glomerular responses to the set of morphed stimuli (Phe/Trp) over time (n = 118 glomeruli in 5 fish). Right: average calcium signal (blue) and s.d. across glomeruli (red) as a function of time. **b**, Correlation coefficient between glomerular input patterns evoked by all different stimuli in the morphing series (Phe/Trp) at different time points. Left: Correlations of population activity pattern before stimulus onset (512 ms before stimulus onset).

Phe/Trp as a function of time (Fig. 13b). No obvious correlation was observable in the pre-stimulus phase (mean correlation coefficient: 0.02 ± 0.16, mean ± SD, at -512 ms). However, correlation between patterns evoked by all possible combinations of stimuli rapidly increases to an average correlation value of 0.91 ± 0.03 (mean ± SD, autocorrelations were excluded from analysis) with onset of the stimulus (t = 256 ms; Fig. 13b). This highly correlated input pattern is stable over time and neither undergoes decorrelation nor shows abrupt transitions between input representations evoked by different odor mixture ratios. This finding is consistent with previous observations showing that Phe and Trp evoke highly overlapping glomerular responses.

Phe/Trp stimuli are known to evoke overlapping MC activity patterns that subsequently become decorrelated (Friedrich and Korsching 1997; Friedrich and Laurent 2001; Friedrich, Habermann et al. 2004; Yaksi, Judkewitz et al. 2007) (n = 156 MCs in 9 OBs). Responses of individual MCs changed in different ways during odor morphing (Fig. 14a, b). Some MC responses changed abruptly

between two stimuli (Fig. 14b, MC 2) while others changed more gradually (Fig. 14b, MC 3) or remained nearly constant (Fig. 14b, MC 1). The mean response of all MCs and the fraction of responsive MCs increased slighly as Phe was morphed into Trp (Fig. 14b, c). The diversity of response transitions is consistent with observations in rat MCs (Khan, Thattai et al. 2008) and indicates that MC activity patterns change in a non-trivial fashion during odor morphing.

I next examined the transition between response patterns across the population of MCs during odor morphing by correlation analysis. As expected, MC activity patterns evoked by all Phe/Trp stimuli were highly correlated shortly after

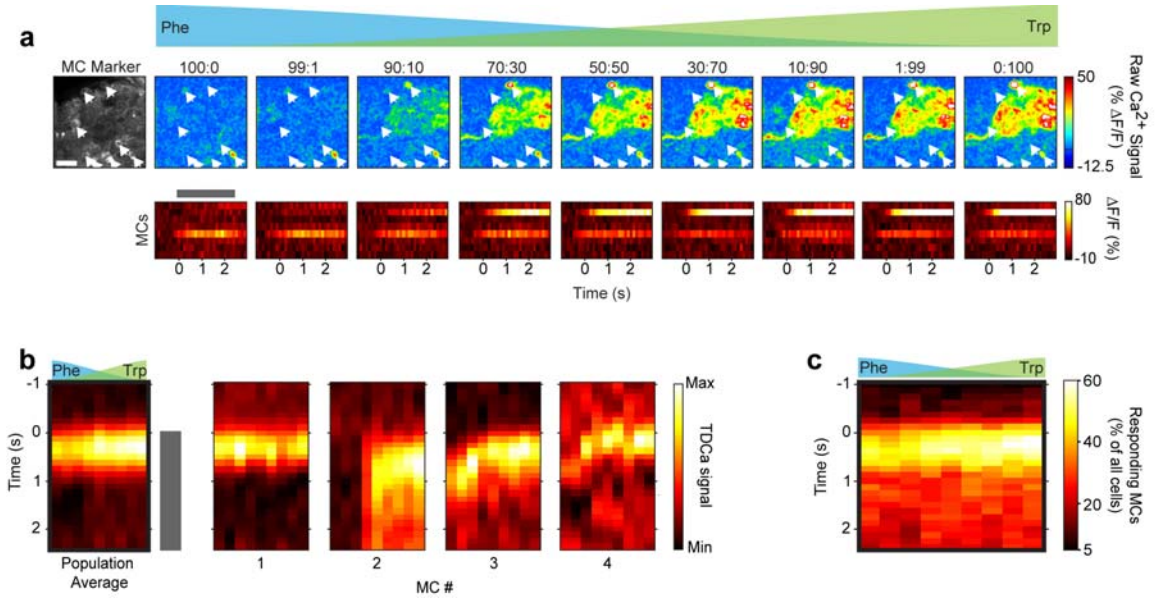

Figure 14 | MC responses to a series of morphed stimuli. a, MC marker expression (left) and time-averaged raw calcium signals evoked by mixtures of Phe and Trp in the ratios indicated on top of the images. Bottom: Evolution of raw calcium signals of MCs indicated by arrows (top) over time (gray bar indicates odor stimulation). Scale bar: 25 µm. **b**, Left: Deconvolved calcium responses (TDCa signals) to the set of morphed odor stimuli averaged over the MC population (n = 156 MCs from 9 OBs). Right: Examples of responses of four individual MCs to the set of stimuli. **c**, Percentage of MCs responding to the stimulus panel as a function of time (threshold for response detection: > 2 s.d. of spontaneous fluctuations).

response onset (Fig. 15a; mean correlation coefficient: 0.80 ± 0.11, mean ± SD, at 256 ms), similar to the corresponding glomerular activation patterns (Fig. 13a, b). Subsequently, response patterns evoked by the pure components became decorrelated (Fig. 15a, lower left and upper right corners) (Friedrich and Laurent 2001; Friedrich, Habermann et al. 2004; Yaksi, Judkewitz et al. 2007).

Interestingly, patterns evoked by intermediate stimuli changed abruptly between the 90/10 and 70/30 mixtures from patterns similar to Phe to patterns similar to Trp at later response times. In the correlation matrix, this switch is represented by two clusters of high correlation coefficients (Fig. 15a) that are separated by a sharp transition (Fig. 15a, bottom, see also Fig. 15d). The mean correlation (± SD) within these clusters was high (0.64 ± 0.02 and 0.77 ± 0.06, at 1280 ms), whereas the mean correlation between clusters was significantly lower (0.27 ± 0.08; $P < 10^{-6}$ for comparison to both clusters; Wilcoxon rank-sum test; Fig. 15a). Euclidean distances were used as a measure for similarity which takes into account the amplitude of the responses. This analysis confirmed the observation made by correlation analysis and also showed sharp transitions between two clusters (Fig. 16a). Moreover, abrupt transitions could be observed at similar positions within the morphing series in different individual fish (Fig. 16b). Correlations of baseline activity do neither show any clear correlation nor any abrupt transitions (Fig. 16c). To finally test whether such relationships between activity patterns can occur by chance I randomly shuffled MC identities for each odor and repeated the correlation analysis. Correlations were always close to zero in these cases indicating that such configurations do not occur by chance (Fig. 16d and Fig. 23b, right). Hence, activity patterns intermediate between Phe and Trp are clearly associated with one of the pure stimuli at the level of OB outputs, but not at the level of OB inputs.

In principal component space, trajectories representing MC response patterns to the first three stimuli in the morphing series were very similar and projected to a clearly defined subvolume (Fig. 15b). Between mixture ratios of 90/10 and 70/30 Phe/Trp, however, trajectories suddenly diverged and projected to a different subvolume. The separation of activity patterns was clearly evident also in principal component analysis performed on time-averaged activity patterns in the steady-state (Fig. 15c).

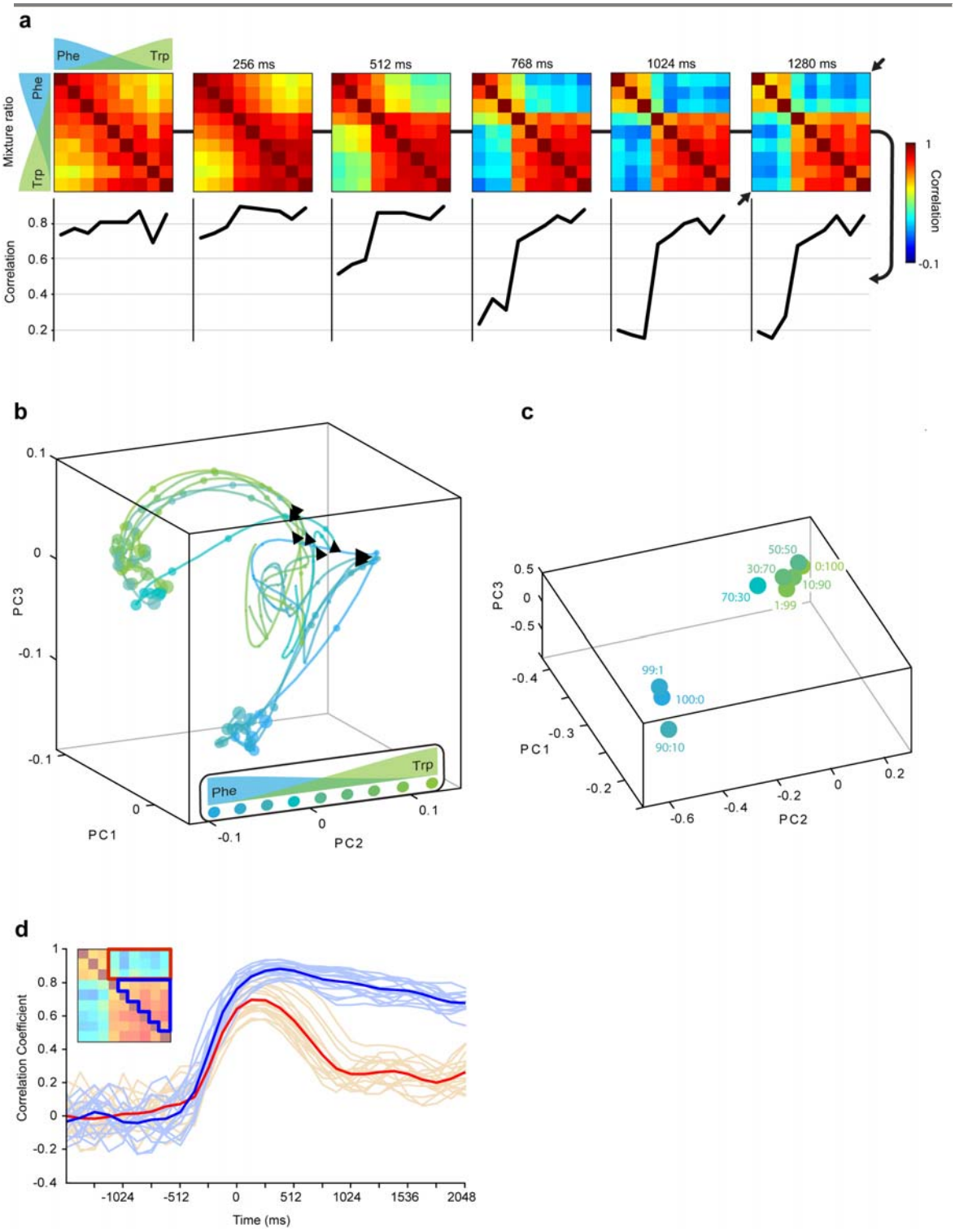

Figure 15 | Multivariate analysis of population activity patterns evoked by morphed similar odors. **a**, Correlation matrices depicting the pairwise correlations between population activity patterns evoked by all morphing stimuli (Phe/Trp) in successive time bins (n = 156 MCs in 9 OBs). Arrows in the corner indicate the correlation between responses to the single odors. Bottom: Sections through the correlation matrices (black line, autocorrelations were interpolated). **b**, Temporal evolution of trajectories representing activity patterns evoked by morphed stimuli in principal component space between -1280 ms and 2304 ms. Conventions as in Fig. 10c. **c**, Steady-state MC activity patterns projected in principal component space (time averaged between 1536 – 2432 ms). **d**, Correlation values of a high-correlation cluster (blue; see inset) and the low-correlation cluster (red) as a function of time. Thick lines are averages.

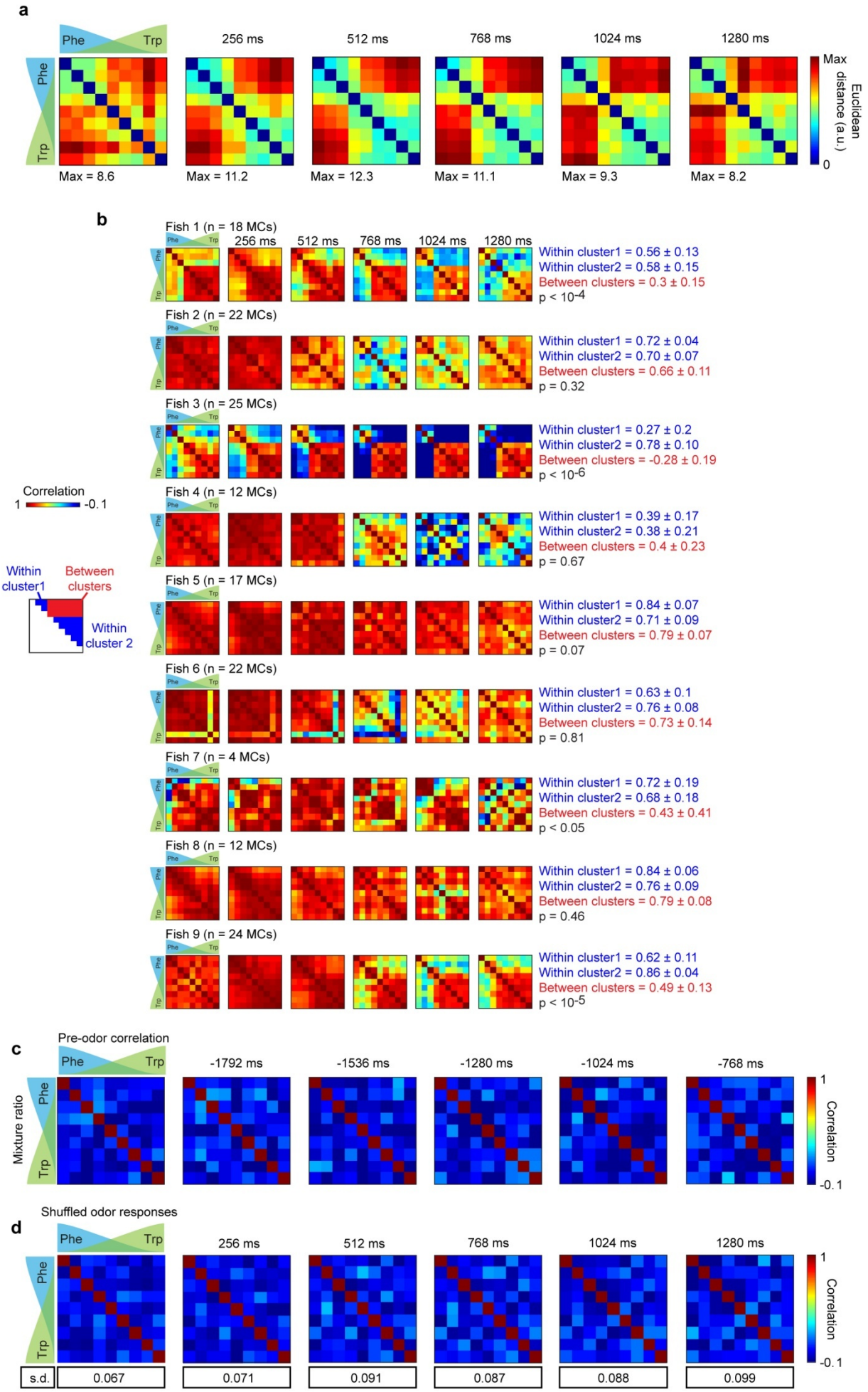
a
Phe
Trp
256 ms
512 ms
768 ms
1024 ms
1280 ms
Max
Euclidean distance (a.u.)
0
Max = 8.6
Max = 11.2
Max = 12.3
Max = 11.1
Max = 9.3
Max = 8.2
b
Fish 1 (n = 18 MCs)
Within cluster1 = 0.56 ± 0.13
Within cluster2 = 0.58 ± 0.15
Between clusters = 0.3 ± 0.15
p < 10-4
Fish 2 (n = 22 MCs)
Within cluster1 = 0.72 ± 0.04
Within cluster2 = 0.70 ± 0.07
Between clusters = 0.66 ± 0.11
p = 0.32
Fish 3 (n = 25 MCs)
Within cluster1 = 0.27 ± 0.2
Within cluster2 = 0.78 ± 0.10
Between clusters = -0.28 ± 0.19
p < 10-6
Correlation
1
-0.1
Fish 4 (n = 12 MCs)
Within cluster1 = 0.39 ± 0.17
Within cluster2 = 0.38 ± 0.21
Between clusters = 0.4 ± 0.23
p = 0.67
Within cluster1
Between clusters
Within cluster 2
Fish 5 (n = 17 MCs)
Within cluster1 = 0.84 ± 0.07
Within cluster2 = 0.71 ± 0.09
Between clusters = 0.79 ± 0.07
p = 0.07
Fish 6 (n = 22 MCs)
Within cluster1 = 0.63 ± 0.1
Within cluster2 = 0.76 ± 0.08
Between clusters = 0.73 ± 0.14
p = 0.81
Fish 7 (n = 4 MCs)
Within cluster1 = 0.72 ± 0.19
Within cluster2 = 0.68 ± 0.18
Between clusters = 0.43 ± 0.41
p < 0.05
Fish 8 (n = 12 MCs)
Within cluster1 = 0.84 ± 0.06
Within cluster2 = 0.76 ± 0.09
Between clusters = 0.79 ± 0.08
p = 0.46
Fish 9 (n = 24 MCs)
Within cluster1 = 0.62 ± 0.11
Within cluster2 = 0.86 ± 0.04
Between clusters = 0.49 ± 0.13
p < 10-5
c
Pre-odor correlation
Mixture ratio
-1792 ms
-1536 ms
-1280 ms
-1024 ms
-768 ms
1
Correlation
-0.1
d
Shuffled odor responses
s.d.
0.067
0.071
0.091
0.087
0.088
0.099

Figure 16 | Euclidean distances, analysis of responses in individual fish and control data sets for Phe/Trp morphing experiments.

a, Euclidean distances between MC activity patterns evoked by morphing of Phe into Trp at successive response times. Scaling maxima of the individual matrices are indicated below. **b**, Correlations between activity patterns across MC populations in individual fish during odor morphing. Average correlation values on the right side of each row (mean ± s.d.) were defined by the blue and red areas indicated at the left side (t = 1280 ms). P-values quantify the statistical significance of comparisons between the mean correlation within high-correlation clusters (clusters 1 and 2; blue areas) and the mean correlation across clusters (red area).**c**, Correlations between baseline activity patterns before stimulus application. **d**, Correlations between activity patterns after randomly shuffling cell identity for each stimulus. The s.d. of correlation coefficients is indicated below the respective matrix (autocorrelations excluded).

Another way to examine the convergence of activity patterns onto distinct representations is to visualize the activity patterns in a metric that represents one state by a value of +1 and another, yet distinct, state by a value of -1. The 2 states were defined in 2 different ways. In one case the states were defined by the activity pattern evoked by the pure components (Phe/Trp, Fig. 17, left). In the other case -1 and +1 was defined as the centers (averages) of the separated groups of evoked activity patterns (100:0 – 90:10 versus 70:30 – 0:100 Phe/Trp, Fig. 17, right). The dimensionality of the data was reduced by extraction of the first principal component (PC). The loadings of the first PC of each time point where then scaled so that -1 and +1 are assigned to the two distinct states. To do so, the two states were normalized by their difference after subtraction of their mean loadings. The resulting values (proximity score) can be infinitive either in positive or negative directions but converge to +1 and -1 when patterns are similar to one or the other state, respectively. Both ways to calculate proximity scores show a clear convergence of Phe/Trp evoked activity pattern onto the discrete states shortly after response onset (Fig. 17). Hence, MC activity patterns change abruptly when Phe is morphed into Trp, implying that neuronal circuits in the OB classify gradually changing inputs into discrete and defined output patterns.

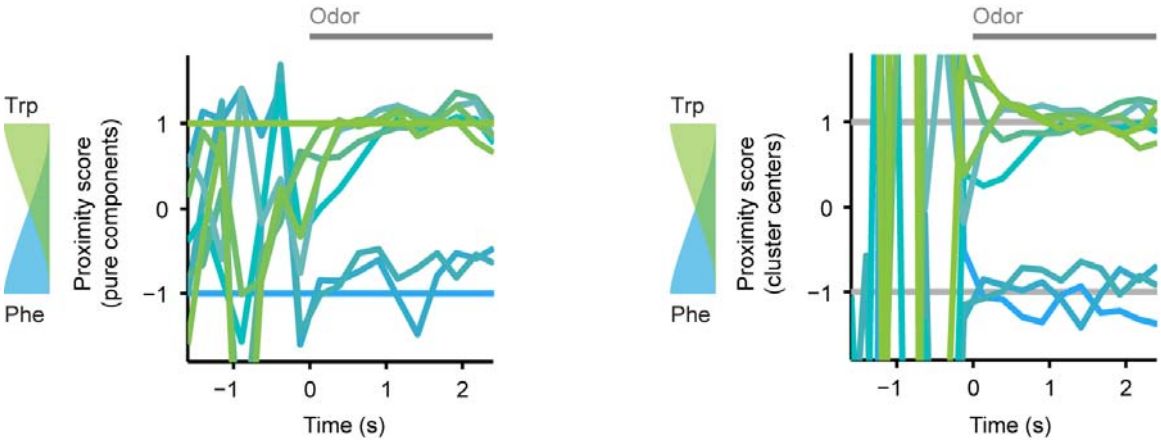

Figure 17 | Further analysis of response transitions during morphing Phe into Trp. Convergence of activity patterns evoked by the morphing series from Phe to Trp onto two independent representations. The two states were assigned to values of +1 and -1 and defined either as the patterns evoked by the two pure odors (left), or as the centroids ("cluster centers", averages) of the separated groups (100:0 – 90:10 versus 70:30 – 0:100 Phe/Trp, right). Only the first principal component was extracted to reduce the dataset to one dimension. For each time point, principal component loadings were scaled by subtracting the mean loading of the two states and normalizing by their difference to assign +1 and -1 to the two different states. The resulting value (proximity score) can vary between positive and negative infinity. The closer the value comes to +1 and -1 the more the activity pattern resembles the one or the other state, respectively. Therefore, for activity patterns evoked by the pure odors these scores are +1 and -1 all the time per definition (left).

I next morphed the odor arginine (Arg, 10^{-5} M) into the dissimilar odor histidine (His, 10^{-5} M) to investigate how glomerular and MC patterns change when the morphing series extends over a greater distance in stimulus space (n = 141 MCs in 7 OBs). Glomerular input patterns evoked by this morphing series changed gradually and remained stable over time. However, input patterns evoked by the pure odors are very dissimilar (n = 159 glomeruli in 5 fish; R = -0.177 at 256 ms, Fig. 18).

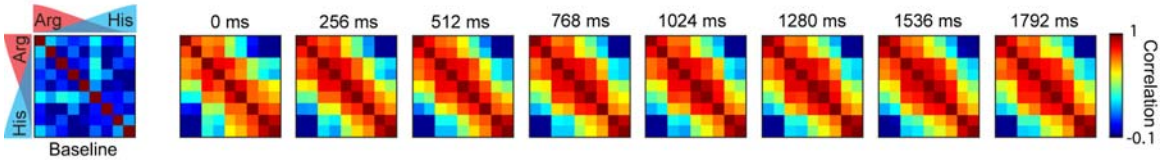

Figure 18 | Glomerular input patterns evoked by dissimilar odors. Correlation coefficients between patterns evoked by morphing of Arg into the dissimilar odor His (n = 159 glomeruli in 5 fish). Left: Pattern correlation of baseline activity before response onset.

In individual MCs odor morphing caused diverse changes in responses as observed for the similar odor pair Phe/Trp (Fig. 19a, b). Some MCs change their firing pattern gradually with changing odor mixtures (Fig. 19b, MC3, MC4), while others show more abrupt changes of their responses (MC1, MC2). The average response of the MC population and the fraction of responding MCs increases at the intermediate mixture ratios between 70/30 and 30/70 (Fig. 19b, c).

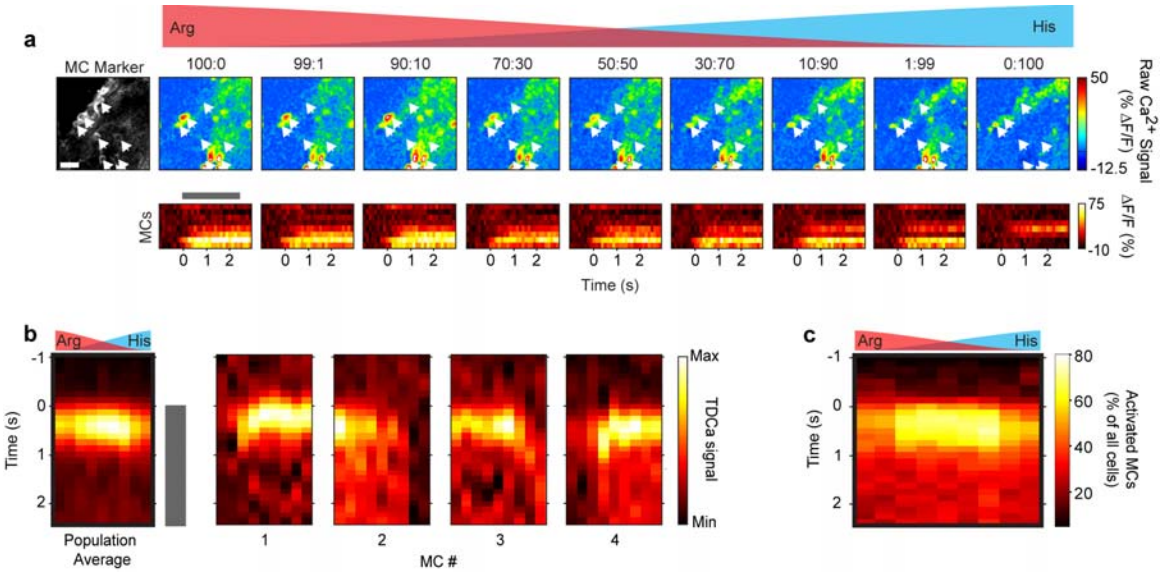

Figure 19 | MC responses to a morphing series of dissimilar odors. a, MC marker expression (left) and time-averaged raw calcium signals evoked by mixtures of Arg and His in the ratios indicated on top of the images. Bottom: Evolution of raw calcium signals of MCs indicated by arrows (top) over time (gray bar indicates odor stimulation). Scale bar: 25 µm. **b**, Left: Deconvolved calcium responses (TDCa signals) to the set of morphed odor stimuli averaged over the MC population (n = 141 MCs from 7 OBs). Right: Examples of responses of four individual MCs to the set of stimuli. **c**, Percentage of MCs responding to the stimulus panel as a function of time (threshold for response detection: > 2 s.d. of spontaneous fluctuations).

Correlation analysis demonstrated that MC population activity patterns evoked by Arg and His (pure odors) were initially dissimilar (R = –0.25 at 256 ms) and remained weakly correlated throughout the odor response (Fig. 20a; arrows), consistent with previous results (Friedrich and Laurent 2001; Yaksi, Judkewitz et al. 2007) and analysis of glomerular input activity (Fig. 18). Patterns evoked by intermediate stimuli during the early response phase became gradually more dissimilar from one component pattern and more similar to the other component pattern, as seen

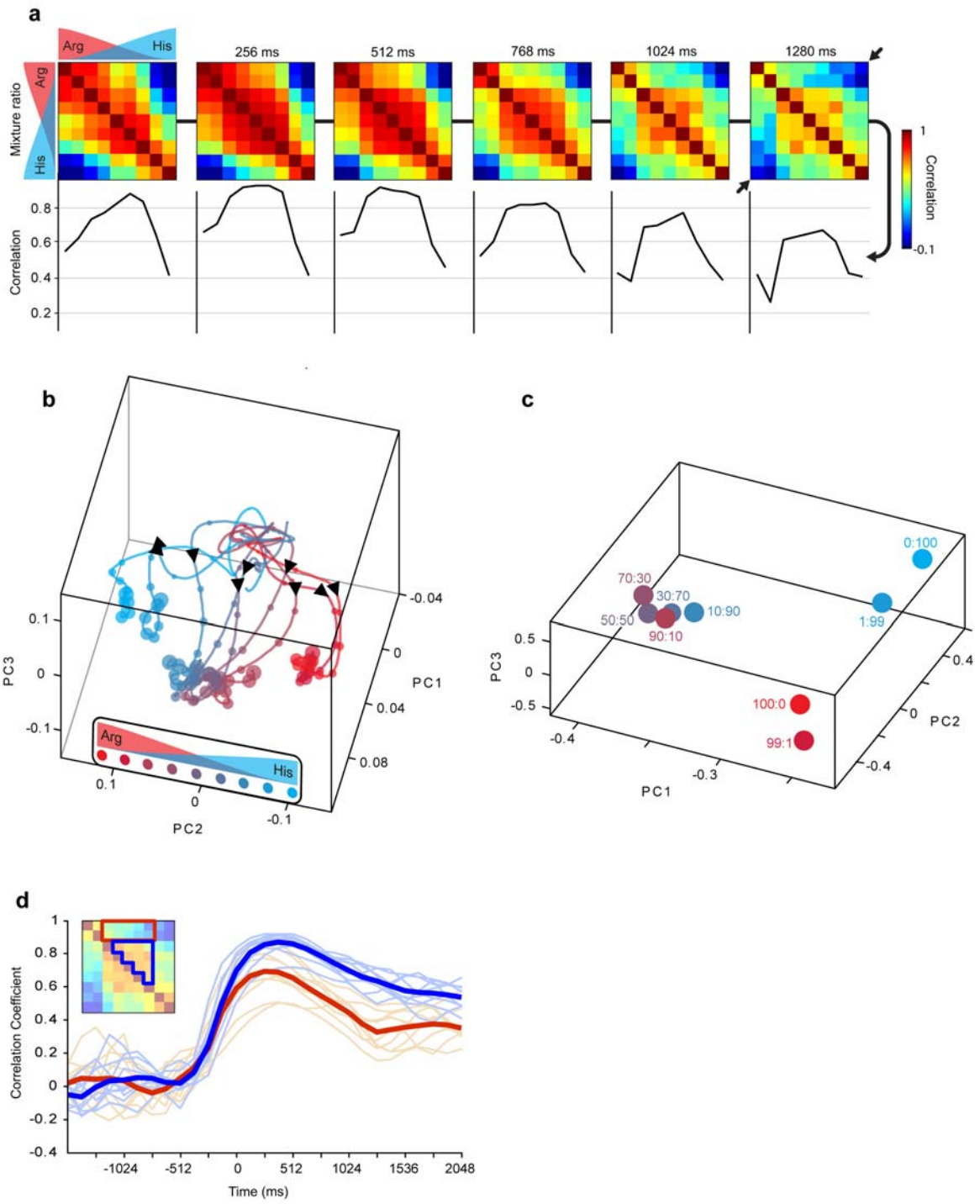

Figure 20 | Multivariate analysis of population activity patterns evoked by morphed dissimilar odors. a, Correlation matrices depicting the pairwise correlations between population activity patterns evoked by all morphing stimuli (Arg/His) in successive time bins (n = 141 MCs in 7 OBs, Arrows in the corner indicate the correlation between responses to the single odors). Bottom: Sections through the correlation matrices (black line, autocorrelations were interpolated). **b**, Temporal evolution of trajectories representing activity patterns evoked by morphed stimuli in principal component space between -1280 ms and 2304 ms. Conventions as in Fig. 10c. **c**, Steady-state MC activity patterns projected in principal component space (time averaged between 1536 – 2432 ms). **d**, Correlation values of the high-correlation cluster (blue; see inset) and the low-correlation cluster (red) as a function of time. Thick lines are averages.

from the continuous band of high correlation coefficients along the diagonal of the correlation matrix (Fig. 20a). Morphing of two dissimilar odors therefore results in a smooth transition between the representations of the pure components during the initial phase of the odor response, similar to the gradual transition between glomerular activation patterns (Fig. 18). Subsequently however, groups of activity patterns became separated from each other. In the center of the correlation matrix a cluster of high correlation coefficients emerged that clearly separated intermediate stimuli from the pure components and the 99/1 or 1/99 mixtures. The mean correlation (± SD) within the cluster was 0.64 ± 0.06, whereas correlations across clusters were significantly lower (0.40 ± 0.12 ; $P < 10^{-4}$, Wilcoxon rank-sum test; 1280 ms). The boundaries of this cluster were clearly defined and remained stable after the initial reorganization of patterns (Fig. 20a, see also Fig. 20d). Similar results were obtained using Euclidean distance as a measure of similarity (Fig. 21a). In addition, abrupt transitions between different states were also observed at the same odor mixture ratios in several individual fish (Fig. 21b). Hence, MC activity patterns evoked by intermediate stimuli become similar to each other but distinct from patterns evoked by both pure components, resulting in three distinct families of odor representations.

Visualization of odor-evoked activity patterns using principal component analysis confirmed these observations (Fig. 20b). Trajectories related to the pure stimuli and the 99/1 or 1/99 mixtures projected to clearly distinct subvolumes. Trajectories evoked by intermediate stimuli, in contrast, converged onto a subvolume that was located in between the subvolumes but separated from both. The separation of these subvolumes was also evident in time-averaged MC activity patterns in the steady-state (Fig. 20c). These results confirm that a gradual change in input patterns results in abrupt changes in output patterns and indicate that population representations of binary odor mixtures can be distinct from the representations of both components.

Taken together, my data suggest that morphing of similar odors leads to abrupt changes between 2 component related representations, while morphing of dissimilar odors also evokes an additional mixture related activity pattern.

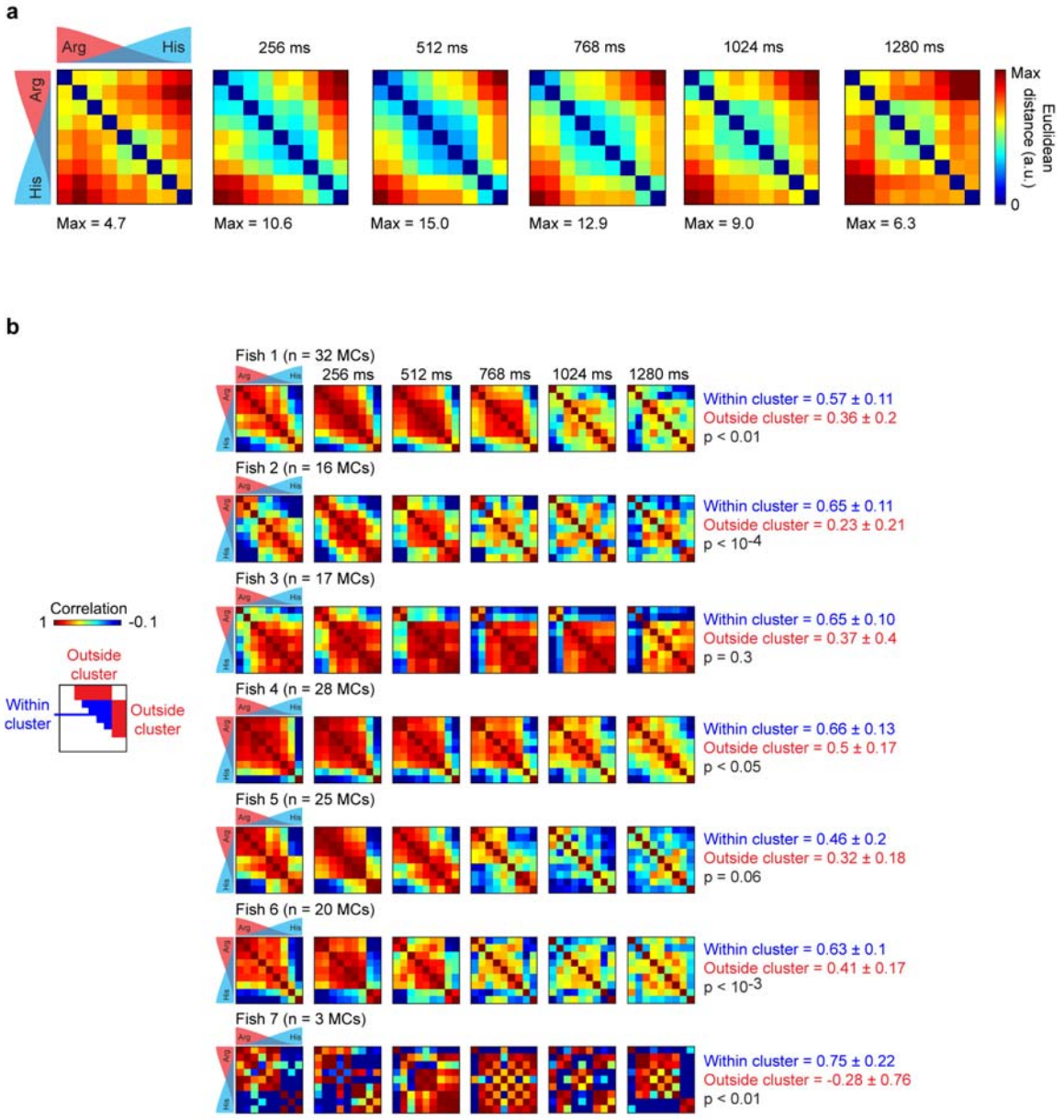

Figure 21 | Euclidean distances and analysis of responses in individual fish for Arg/His morphing experiments.

a, Euclidean distances between MC activity patterns evoked by morphing Arg into His at successive response times. Scaling maxima of the individual matrices are indicated below. **b**, Correlations between activity patterns across MC populations in individual fish during odor morphing. Average correlation values at the right of each row (mean ± s.d.) were defined by the blue and red areas indicated at the left side (t = 1280 ms). P-values quantify the statistical significance of comparisons between the mean correlation within high-correlation clusters (blue area) and the mean correlation across clusters (red areas).

However, it remains unclear whether the OB always separates similar input patterns into 2 distinct representations and dissimilar input into 3 representations. Moreover, it would be interesting to investigate whether both pattern separation strategies can be observed within the same population of MCs. These questions were addressed by an additional set of experiments. Within the same animals I morphed the odor tryptophan (Trp) into the similar odor tyrosin (Tyr) through a series of intermediate mixtures (100/0, 75/25, 50/50, 25/75, 0/100). Tyr, in turn, was morphed into the dissimilar odor alanin (Ala). Correlation analysis of the complete morphing series (Trp-Tyr-Ala) showed a high initial correlation between

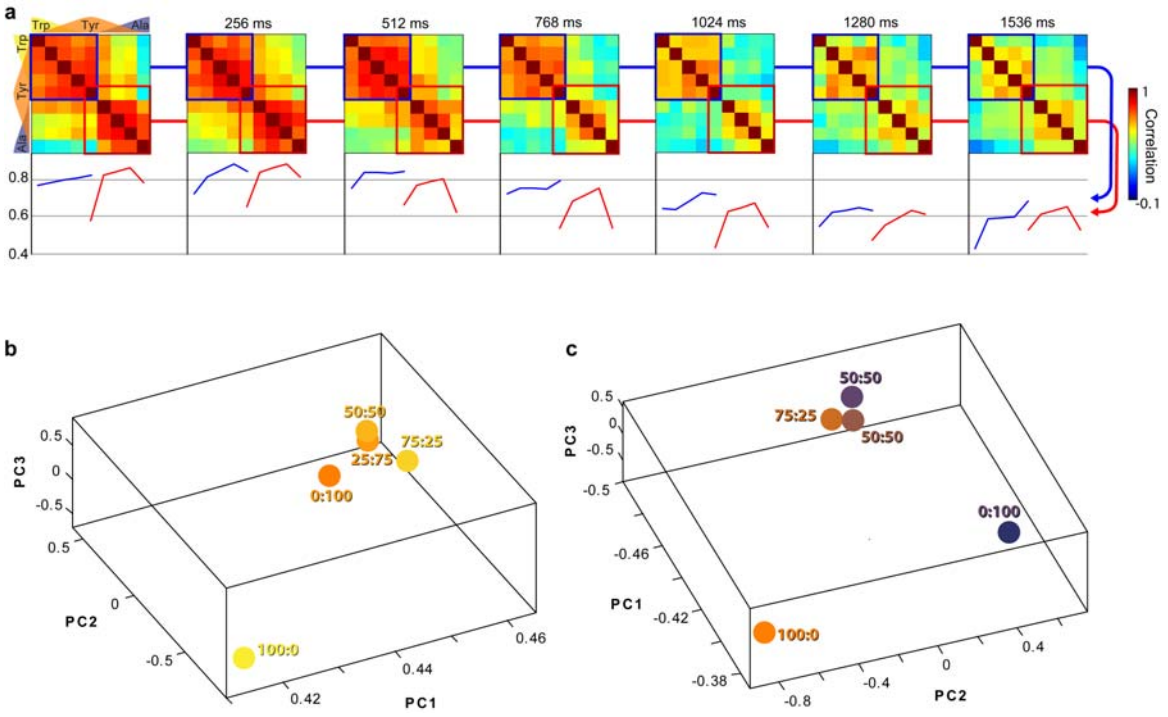

Figure 22 | Correlation and principal component analysis of control experiments.
To control whether similar odors are always separated into two representations and dissimilar odors always become separated into 3 clusters we repeated the morphing experiments with a different set of odors. Trp was morphed into the similar odor Tyr in the steps 100/0, 75/25, 50/50, 25/75, 0/100 (Trp/Tyr). Likewise, the odor Tyr was morphed into the dissimilar odor Ala. Both morphings have been performed during the same set of measurements. **a**, Time series of correlation matrices depicting pairwise similarity between activity patterns evoked by all stimuli in successive time bins (n = 99 MCs in 6 OBs). Blue square: Correlations between the similar odors Trp and Tyr, Red square: Correlations between the dissimilar odors Tyr/Ala. Bottom: Sections through correlation matrices at the position indicated by the line (blue: Trp/Tyr, red: Tyr/Ala; autocorrelations were replaced by interpolated values). **b**, MC activity patterns in principal component space related to the similar odor pair Trp/Tyr, time-averaged during the steady-state (1408 – 2048 ms). **c**, Same as in b but for the dissimilar odor pair Tyr/Ala.

patterns evoked by all stimuli within the Trp/Tyr morphing steps at an early time point (Fig. 22a, blue square). Likewise, patterns evoked by Tyr/Ala mixtures were also highly correlated during the initial phase of the response (Fig. 22a, red square). At later time stages (1280 ms – 1536 ms), Trp/Tyr evoked responses formed 2 clusters with a transition between the mixture ratios 100/0 and 75/25, while Tyr/Ala related activity patterns formed a central cluster between 75/25 and 25/75 which was only weakly correlated to the response patterns evoked by the components (Fig. 22a). This finding was confirmed by principal component analysis of the activity patterns averaged over the steady-state (Fig. 22b, c). Trp/Tyr evoked patterns showed a clear separation of clustered representations in principal component space between 100/0 and the remaining stimuli (Fig. 22b). In contrast, the dissimilar odors Tyr/Ala evoked three distinct steady-states. Two states represent the pattern evoked by the pure components Tyr and Ala (100/0 and 0/100) while activity patterns evoked by intermediate mixtures (75/25, 50/50 and 25/75, Tyr/Ala) form a third cluster in principal component space (Fig. 22c).

To confirm the significance of my results I randomly selected 50% of the MCs in each dataset and repeated the correlation calculation and principal component analysis with these subsets of cells (Fig. 23 a-c). For each data set this control was repeated 10 times (see also Fig. 23b, c, right). Results from different MC subsets were similar to each other and to the full data set.

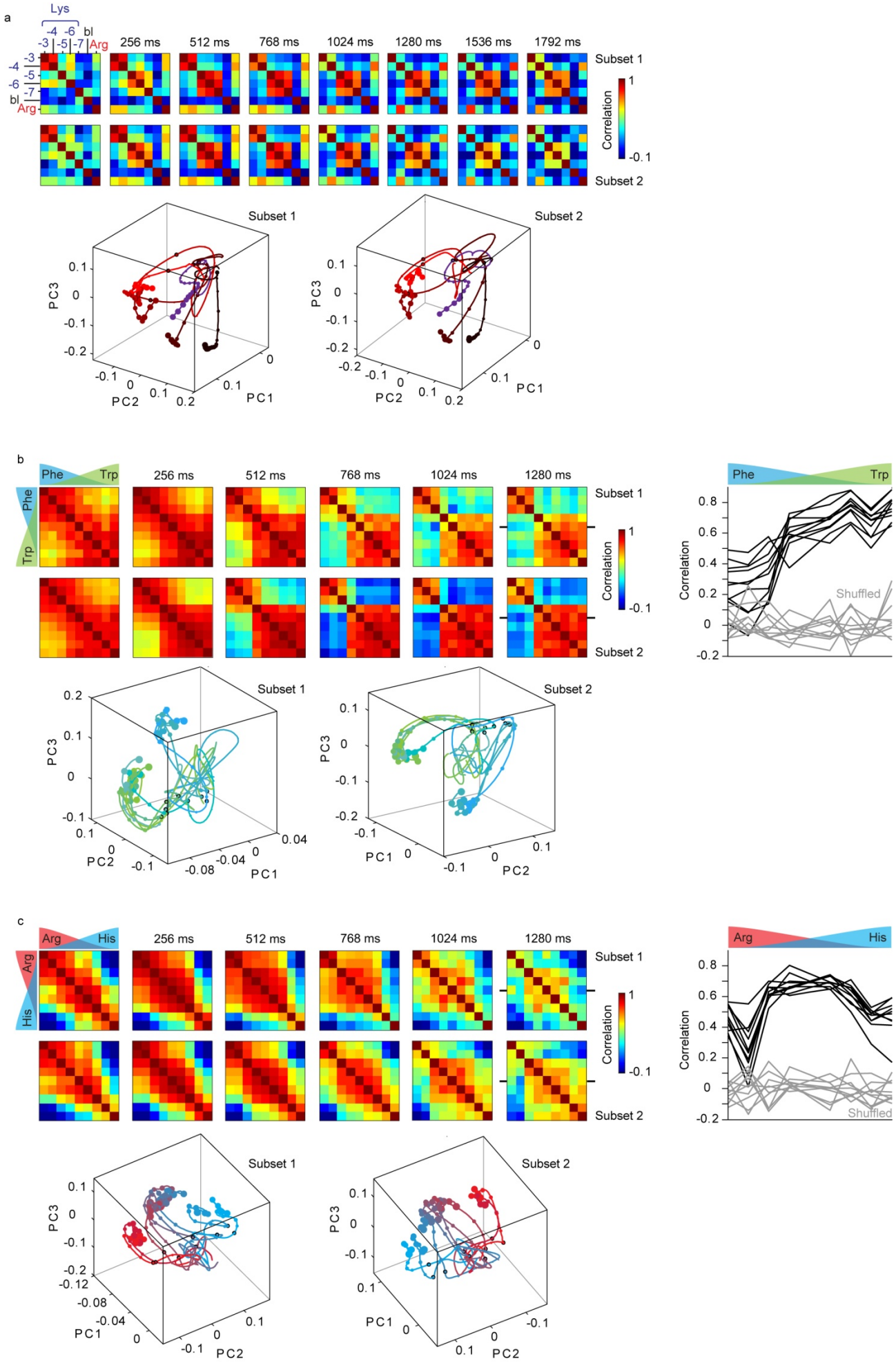
a
Lys
-4 -6 bl
-3 -5 -7 Arg
256 ms
512 ms
768 ms
1024 ms
1280 ms
1536 ms
1792 ms
Subset 1
Correlation
1
-0.1
Subset 2
Subset 1
Subset 2
PC1
PC2
PC3
b
Phe
Trp
256 ms
512 ms
768 ms
1024 ms
1280 ms
Subset 1
Subset 2
Correlation
Shuffled
c
Arg
His
256 ms
512 ms
768 ms
1024 ms
1280 ms
Subset 1
Subset 2
Correlation
Shuffled

Figure 23 | Repetition of analysis using randomly reduced data sets. Correlation analysis and principal component analysis were performed on randomly selected subsets of MCs, each containing 50 % of all MCs in a data set. This procedure was repeated 10 times for each data set. **a**, Top: Correlation analysis of responses evoked by different concentrations of Lys and the control odor Arg in two randomly selected subsets of MCs, each containing half of the MCs (n = 70 out of the 140 MCs). Bottom: Trajectories in principal component space representing response patterns in the two random subsets of MCs as a function of time. **b**, Same analysis for activity patterns evoked by the Phe/Trp morphing stimuli for two random subsets of MCs (n = 78 MCs out of 156 MCs in total). The cross-section through the correlation matrices (position indicated by black lines in correlation matrices) of the 10 repetitions of this analysis are shown on the right (black lines) for the time point 1280 ms. Autocorrelations were interpolated. Gray lines show cross-sections through correlation matrices after random shuffling of cell identity (see Fig. 16d). **c**, Same analysis for the Arg/His dataset (n = 70 MCs out of 141 MCs). The cross-section through the correlation matrices (position indicated by black lines in correlation matrices) of the 10 repetitions of this analysis are shown on the right (black lines) for the time point 1280 ms.

Pattern classification is mediated by coordinated responses of mitral cell subsets

I next asked how abrupt transitions between discrete representations can arise in population activity from diverse response profiles of individual MCs to a morphing series. One possibility is that transitions between activity patterns are driven by subsets of MCs whose responses change in a coordinated fashion at the transition point. To test this hypothesis, I represented responses of each MC to the morphing series in a given time window (768 ms after response onset) by a 9-dimensional vector and subtracted the mean. These response profiles were combined into a response matrix representing the centered responses of all MCs (rows) to all stimuli (columns). MC responses were then ranked by decreasing covariance of each MC response profile with a template representing the transition point. Response profiles that closely follow the transition are therefore located at the top of the matrix while inverted response profiles appear at the bottom. The central region of the matrix contains responses that are uncorrelated to the pattern transition or do not change much during morphing.

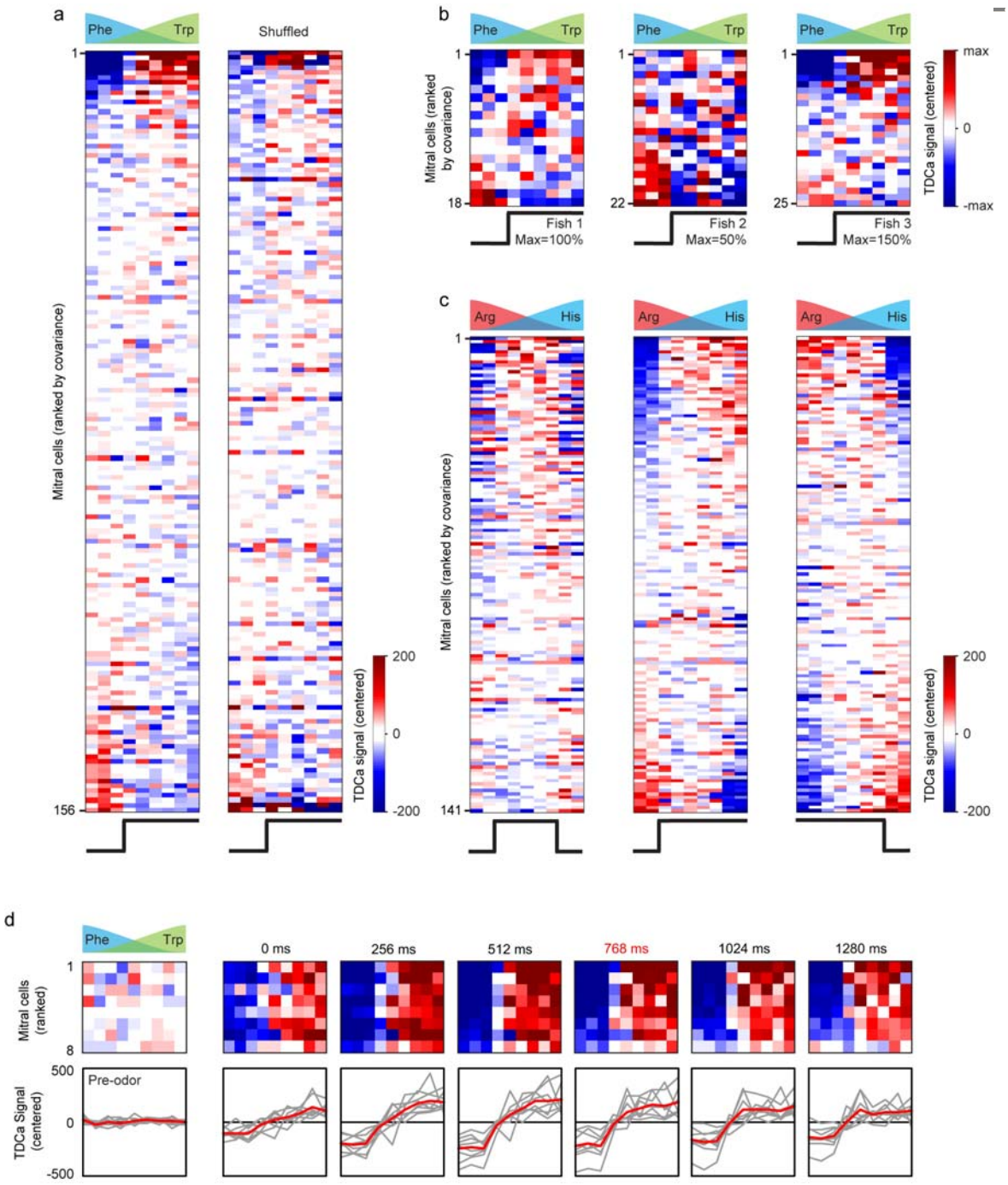

Figure 24 | Subsets of mitral cells show abrupt response transitions during odor morphing
a, Left: Matrix for all MC responses at 768 ms (n = 156 from 9 fish) to the different morphing steps of similar odors (Phe/Trp). Responses were mean subtracted and sorted with respect to the decreasing covariance of the response profiles with a fixed template (bottom) defined by the transition point in the population activity (see Fig. 15a, bottom). Right: Same as (a) after shuffling of stimulus identities for each MC. **b**, Same as (a) but for 3 individual fish. Scaling maxima are indicated below **c**, Left: matrix of all MC responses (n = 141 from 7 fish) at 768 ms to Arg/His. MCs are sorted by the decreasing covariance of the response profiles with a template representing 2 response transitions (see Fig. 20a, bottom). Center, right: same as (a) but with a template defining both response transitions separately **d**, Top: Response profiles of the eight MCs with highest covariance with the template of (a) at 768 ms as a function of time. Indices of MCs are the same at all time points. Bottom: response profiles of individual MCs (gray line) and mean response (red line) over time as line plots. Left: before response onset.

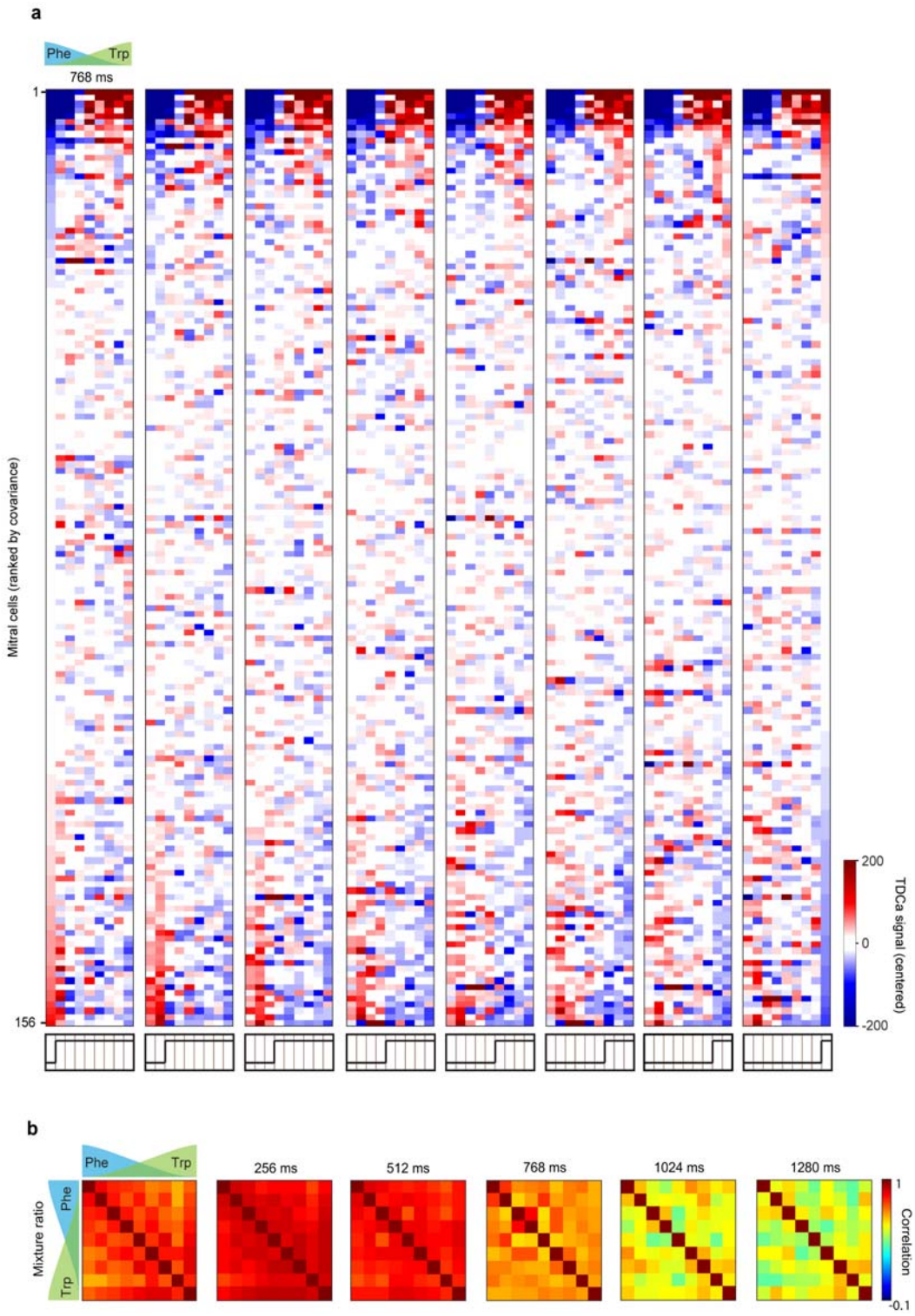

Figure 25 | Abrupt transitions in mitral cell subsets are responsible for switching representations in population activity patterns a, Matrix for all MC responses at 768 ms (n = 156 from 9 fish) to morphing of similar odors (Phe/Trp). Responses were mean subtracted and sorted in accordance with the decreasing covariance of the response profiles with different templates (bottom) **b**, Correlation matrices for MC activity patterns evoked by morphing of Phe into Trp after removing the 10 % of MCs showing the highest absolute covariance with the template in Fig. 24a.

For the morphing series of Phe into Trp, the template changed from zero to one at the transition point between 90/10 and 70/30 Phe/Trp (Fig. 24a, in accordance with Fig. 15 a, bottom). A substantial fraction of MC response profiles showed no obvious relationship to the template (Fig. 24a; central part of the matrix) but sharply defined transitions occurred in a subset of MCs (top and bottom part of the matrix). Among these MCs, the change point was aligned remarkably well to the transition between 90/10 and 70/30. This type of response transitions was observed in individual fish as well (Fig. 24b). Moreover, aligned response transitions did not change dramatically when the transition point in the template was varied showing that response transitions usually occur between 90/10 and 70/30 Phe/Trp (Fig. 25a). In addition, the transition point became much less pronounced after shuffling of stimulus identities (Fig. 24a, right), showing that the alignment of response transitions does not simply occur by chance. The sharp transition between MC response patterns (Fig. 15a) was completely abolished when the 10 % of MCs showing the most pronounced transitions (highest absolute covariance with the template) were removed from the data set (Fig. 25b). The abrupt transition between population activity patterns can therefore be attributed to coordinated response changes across a relatively small subset of MCs. MC responses that changed abruptly during the later phase of the odor response changed more gradually shortly after response onset (Fig. 24d). Hence, abrupt transitions between activity patterns do not emerge because additional, specific MCs are recruited over time but because a subset of MC responses becomes more sharply tuned to the transition.

I next examined how multiple transitions between population activity patterns occur when Arg is morphed into the dissimilar odor His (n = 141 MCs from 7 fish). I first designed a template that changed from zero to one between 99/1 and 90/10 Arg/His and back to zero between 10/90 and 1/99 Arg/His, thus representing both transition points in the population response (Fig. 24c, left). In the response matrix, abrupt response changes in a subset of MCs were evident at each transition point. Some MC responses changed at both transition points, while other responses changed only at the first or at the second transition point. These two subpopulations of MCs could be extracted independently by templates representing only the first or the second transition (Fig. 24c, center and right).

Transitions between multiple discrete output patterns are therefore mediated by coordinated response changes among different, yet partially overlapping, MC ensembles.

In order to categorize and quantify the response profiles of individual MCs for the different data sets, I performed fitting analysis as used before in other studies (Leutgeb, Leutgeb et al. 2005; Khan, Thattai et al. 2008). To this end, MC responses to a series of stimuli (concentration- or mixture series) where fitted to sigmoid, linear and quadratic functions respectively (Fig. 26a). If MC responses change gradually with stimulus changes the best fit would be a linear function. In

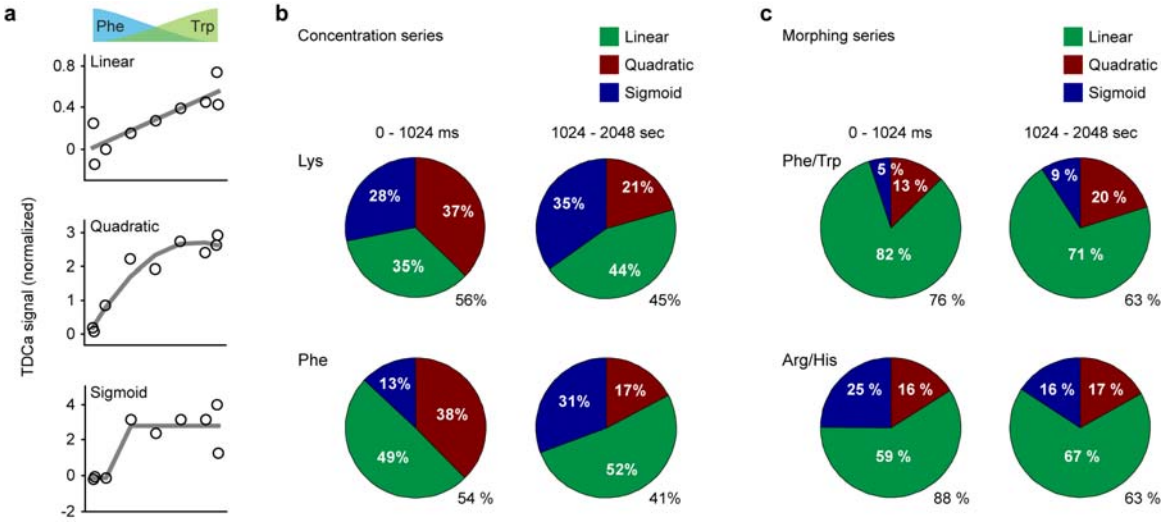

Figure 26 | Fit of mitral cell response profiles to linear, quadratic and sigmoid functions. Response profiles across the morphing series of all MCs were fitted by a linear, quadratic or sigmoid function. MCs for which none of the fits was significant ($P > 0.05$) were excluded from the analysis. Remaining MCs were assigned to the fit (linear, quadratic or sigmoid) which explained most of the variance (highest F-statistics, see Methods for details). **a**, Examples of responses of individual MCs to changes in odor mixture ratios (Phe/Trp) fit by linear, quadratic and sigmoid functions. **b**, Fraction of MC responses to different concentrations of Lys (n = 140 MCs from 4 OBs; top) and Phe (n = 128 MCs from 7 OBs; bottom) that were best fit by linear (green), quadratic (red) and sigmoid (blue) functions. The fraction of MCs fitted significantly ($P < 0.05$) is indicated at the lower right, respectively. Analyses were performed for averaged time periods during the responses (0 – 1024 ms (left) and 1024 – 2048 ms (right) after response onset **c**, Fraction of response profiles obtained during morphing of Phe into Trp (n = 156 MCs in 9 OBs; top) and Arg into His (n = 141 MCs in 7 OBs; bottom) that were best fit by linear (green), quadratic (red) and sigmoid (blue) functions. Conventions as in (b).

case of a more abrupt response transition, a sigmoid function would be a more accurate fit for the MC response profile. Other forms of transitions or responses that have their maximum at intermediate stimuli would be described best by quadratic functions. If at least one of the three fitting functions provided a significant fit, the MC was assigned to the fitting function which explained most of the variance in the response profile. This analysis was done for response profiles averaged over two time periods during the response, an early period (0-1024 ms) and a late period (1024-2048 ms). In almost all data sets, the number of sigmoid response transitions increased in the second time period of the response (Fig. 26b, c). This indicates a sharpening of initially more gradual responses during the first 2 seconds of the responses. However, it is difficult to compare response transitions during changes in odor concentration to those evoked by mixtures interactions since both might be based on different mechanisms.

Discussion

Summary

TDCa imaging of odor responses in zebrafish revealed that MC activity patterns are surprisingly stable across odor concentrations but sensitive to changes in the molecular identity of an odor. This indicates that the OB is capable of generalizing over a large range of odor concentrations but separates representations evoked by different odors. On the other hand, gradual variations in odor identity and glomerular input patterns lead to abrupt transitions between MC population activity patterns at later time stages of the response. Activity patterns evoked by morphing of similar odors were alike patterns evoked by either one or the other component without any intermediate representation. In contrast, mixtures of dissimilar odors activated an intermediate representation which was only weakly correlated with the activity patterns evoked by the odor components alone. For both types of odor mixtures computations were driven by coordinated response changes among small MC ensembles. Hence, the OB classifies input patterns into discrete and defined outputs. This classification is reminiscent of attractor networks, creates robustness against noise, and may be involved in the generation of perceptual phenomena such as odor masking and configural odor perception.

Concentration-invariance of odor representations in the OB

How does the brain construct concentration-invariant odor representations from concentration-sensitive sensory inputs? Consistent with observations in other species, I found that concentration-response functions of individual MCs are diverse (Fig. 8b, Fig. 9b, Fig 26b; see also (Stewart, Kauer et al. 1979; Wellis, Scott et al. 1989; Scott, Wellis et al. 1993; Laurent, Stopfer et al. 2001; Bathellier, Buhl et al. 2008)) yet population activity patterns evoked by the same odor are similar within a certain concentration range (Stopfer, Jayaraman et al. 2003) (Sachse and Galizia 2003; Bathellier, Buhl et al. 2008). Hence, concentration-dependent changes in the responses of individual MCs do not occur in unison and cause only small changes in the population response. Moreover, my results

demonstrate that MC activity patterns evoked by different concentrations of the same odor remain clustered during the dynamic phase of the odor response, whereas representations of molecularly different stimuli are actively separated. As a consequence, odor representations across OB output neurons become sensitive to changes in molecular structure but partially invariant to odor concentration.

Even though MC activity patterns evoked by different concentrations do not undergo decorrelation, they exhibit small differences. OB output activity patterns therefore contain some information about odor concentration that may be used by higher brain areas, for example, to evaluate stimulus intensity. Nevertheless, my results suggest that odor representations in the OB become optimized to represent odor identity rather than intensity. Consistent with this notion, many animals can discriminate between closely related molecules but generalize over a range of concentrations (Abraham, Spors et al. 2004; Valentincic, Miklavc et al. 2005; Cleland, Johnson et al. 2007; Uchida and Mainen 2007). For example, mice can learn to make accurate discriminations between very similar odors but have difficulties to distinguish concentrations (Abraham, Spors et al. 2004). Interestingly, changing odor concentration beyond the range of stable representations could result in abrupt pattern transitions (e.g., between 10^{-5} and 10^{-4} M Lys; Fig. 10). Likewise, the perceived identity of an odor can change suddenly at a certain threshold concentration (Gross-Isseroff and Lancet 1988; Laing, Legha et al. 2003). Together, these results suggest that the first processing steps towards concentration-invariance of odor recognition occur already in the OB. Moreover, it also shows that the basic pattern classification strategies – pattern generalization and pattern separation – are realized within the same processing stage of the neuronal hierarchy.

Pattern separation in the OB

To investigate the dynamics of pattern separation in the OB in more detail, one odor was morphed into another. Morphing experiments revealed that gradual changes in the molecular identity of odors are reflected in highly correlated gradual changes of glomerular input patterns in the OB. The same gradual

transitions were also observed in the initial representations of morphed odors in MC populations as expected (Friedrich and Laurent 2001; Yaksi, Judkewitz et al. 2007). However, after the dynamic phase of the odor response transitions between MC activity patterns became abrupt, switching either between 2 or 3 distinct representations. The “coding space” encompassing all possible MC activity patterns is therefore discontinuous, consisting of relatively stable regions that are separated by instable transition regions. These findings are fully consistent with predictions from attractor networks, as illustrated schematically in Fig. 27. My results therefore provide strong evidence that neuronal circuits in the OB classify glomerular input patterns into discrete and defined outputs in an attractor-like fashion.

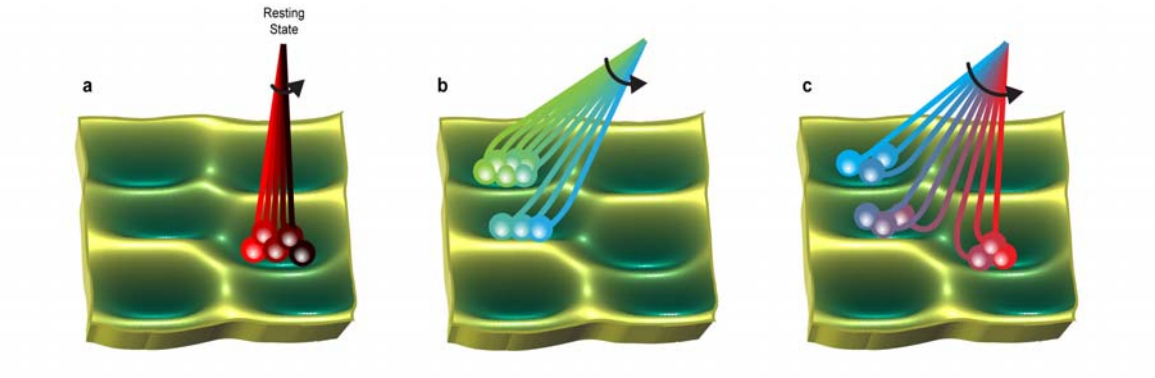

Figure 27 | Schematic illustration of pattern classification effects. Responses evoked by different odor stimuli are represented by trajectories that start from a common resting state into different directions in the representational space; local minima in the landscape represent stable states. **a**, Similar stimuli (e.g. same odor at different concentrations, small angular separation) converge into the same local minimum as long as their variation occurs along a dimension where minima are broad and response changes do not exceed a particular theshold. In this case patterns are not separated, as observed for MC responses to different concentrations. **b**, If the difference between input patterns becomes stronger (larger angular separation) activity patterns become separated into two different states (local minima), consistent with the abrupt switch of MC representations during morphing of similar odors. **c**, Trajectories converge into three different local minima if stimuli are morphed over a larger distance in input space (large angular separation) This is consistent with multiple pattern transitions during morphing of dissimilar odors in this study.

Pattern transitions were mediated by response changes among relatively small subsets of MCs, rather than by global switches in activity levels. These MC ensembles nevertheless had a strong impact on OB output patterns because their responses changed in a coordinated fashion near the transition points in the population data, even in different animals. Abrupt transitions between odor representations are therefore a population phenomenon that is less obvious when MC responses are analyzed individually. This may account for the fact that discrete pattern classification has not been detected by an analysis of individual MC responses in rats (Khan, Thattai et al. 2008). However, fitting analysis of our MC data revealed similar statistics for single cell response profiles during odor morphing as observed in this study.

Interestingly, basic effects of pattern classification (Fig. 27) exhibit parallels to different perceptual phenomena. As discussed above, the separation of coding space into discrete regions results in a limited stability of odor representations against changes in some stimulus variables, which might be involved in concentration-invariant odor perception (Fig. 27a) (Abraham, Spors et al. 2004; Valentincic, Miklavc et al. 2005; Cleland, Johnson et al. 2007; Uchida and Mainen 2007). Moreover, weak background odor is usually not perceived in the presence of a stronger foreground odor (masking) (Valentincic, Kralj et al. 2000). Likewise, the population response to a high-concentration odor (“foreground”) remains stable when a low concentration of another odor (“background”) is blended in, until a sudden switch occurs (Fig. 27b). In addition, binary mixtures of odors can be perceived as distinct from their components, and MC activity patterns evoked by binary mixtures can become separated from the representations of both pure odors (Fig. 27c) (Valentincic, Kralj et al. 2000). I therefore propose that odor perception reflects, at least to some extent, discrete pattern classification in the OB.

Abrupt transitions between MC activity patterns are consistent with predictions from attractor networks. Odor classification by attractor networks has been proposed to occur in the mammalian OB based on multisite electroencephalogram recordings of oscillatory population activity (Freeman and Grajski 1987). My data, in contrast, represent firing rate changes across

individual MCs. It therefore remains unclear how these models relate to my results. Clear evidence for attractor-based pattern classification exists in the hippocampus, where the activity of a majority of place cells can change abruptly during morphing of familiar environments (“global remapping”) (Wills, Lever et al. 2005; Colgin, Moser et al. 2008). Contrary to the OB, the hippocampus contains abundant excitatory connections between principal neurons which are thought to be important for pattern completion (Treves and Rolls 1994; Colgin, Moser et al. 2008). My results therefore demonstrate that a neuronal circuit dominated by inhibition can also classify inputs in an attractor-like fashion, consistent with theoretical studies (Xie, Hahnloser et al. 2002; Machens, Romo et al. 2005). However, in contrast to pattern completion in the hippocampus the OB rather performs the opposite computation. Initial representations in MC populations are usually “overcomplete” rather than “incomplete” and activity patterns become sparser during overlap reduction by pattern reorganization.

Although pattern classification in the OB resembles the behavior of attractor networks, at least three issues should be considered. First, an odor drives the system from a common resting state towards a ”steady-state” pattern that exists only for the duration of the stimulus. Hence, the system is actively “driven”, rather than passively “attracted”, towards an output pattern. Second, experimental data show that activity patterns in the steady state change less rapidly than during the initial phase of the odor response (Fdez Galan, Sachse et al. 2004; Friedrich and Laurent 2004; Mazor and Laurent 2005) but it cannot be determined with certainty that this state is indeed stable. Third, odor representations are not sharply delineated in all dimensions because transitions between families of patterns are mediated only by subsets of MCs.

Functional implications of pattern classification

The discretization of coding space associated with pattern classification has important consequences for neuronal processing. First, it imposes a limit on the resolution of sensory coding because similar inputs may not become separated even if they are, in principle, distinguishable. A system with high resolving power

such as the OB thus requires a large number of possible output states. Unless the number of neurons is very large, output patterns may therefore not be orthogonal to each other and separated by relatively low thresholds, consistent with my observations in the OB.

Second, the classification of inputs into discrete outputs can eliminate variations between input patterns that convey the same message. Such variations can, for example, arise from background odors or neuronal noise. Noise tolerance increases, but resolution decreases, with the stability range of output patterns

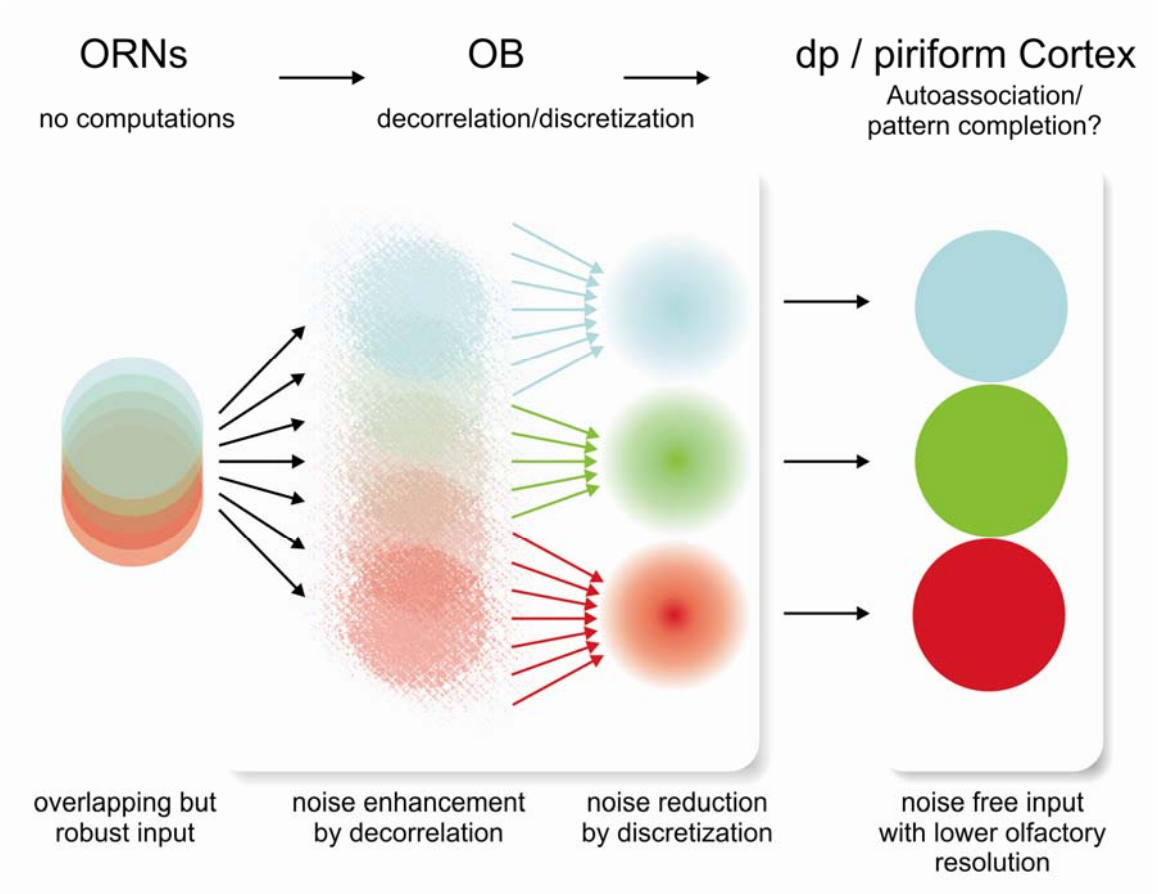

Figure 28 | Potential functional implications of discrete pattern classification. ORN responses are very robust but can be highly overlapping (left). These input overlaps are transmitted to the MCs in the OB. Decorrelation in the OB enhances differences in activity patterns but also increases the neuronal noise. Discretization reduces noise on the cost of olfactory resolution (middle). This noise reduced and non-overlapping output from the OB is required in higher brain areas since further computations might involve noise-sensitive pattern completion mechanisms (right).

(Fig 28, middle). Pattern classification therefore balances the resolution of sensory representations against noise tolerance (Fig. 28).

Third, classification strategies may be adapted to filter irrelevant information out of input patterns. For example, non-isotropic classification filters could separate some inputs but generalize over others (Fig. 27a, b), as observed for odors that differ in molecular structure and concentration, respectively.

Fourth, the main target area of the OB, the piriform cortex (dorsal posterior telencephalon in zebrafish (Wullimann and Mueller 2004; Yaksi, von Saint Paul et al. 2009)), has been proposed to function as an autoassociative memory network that requires decorrelated and noise-limited input patterns (Hasselmo, Wilson et al. 1990; Barnes, Hofacer et al. 2008). Pattern classification in the OB may therefore be an important pre-processing step for subsequent pattern separation and completion operations in cortical areas (Fig. 28).

In general, the classification of complex information into categorial outputs is important not only in sensory systems but also for brain areas concerned with memory formation, decision making and other tasks.

Outlook

Several interesting questions arise by the outcome of this study. First of all it would be interesting to investigate the read out and interpretation of OB output in higher olfactory brain areas using the same methods and stimuli as used in this study. Since higher brain areas have – in theory – access to all different time periods during the response it would be particularly interesting which time slice is read out and further processed by higher olfactory areas. If early olfactory information is used for the formation of representations in higher brain areas a more gradual transition between representations would be expected. In contrast, if later time stages of the odor response are used this should be reflected in more abrupt transitions between different representations. Since this information would be expected to influence the decision and behavior of animals it would further be invaluable to study the perceptual consequences of odor morphing and concentration changes in behaving animals. Even though several behavioral

correlates of my results have been described earlier such as concentration invariance (Abraham, Spors et al. 2004; Valentincic, Miklavc et al. 2005; Uchida and Mainen 2007) and odor masking (Valentincic, Kralj et al. 2000), it remains unclear whether abrupt state transitions evoked by morphed odors also manifest in the behavior of the animal at the same odor mixture ratios as measured in the neuronal population. Moreover, an animal could be forced to make decisions at earlier and later time points during the response and it could be investigated whether behavioral transitions are more gradual at earlier time points and more abrupt at later time stages. If so, this rather correlative “bottom-up” approach could then be complemented by more causal “Top-down” investigations. It would be interesting to test if the profiles of response transitions can be manipulated by any means, e.g. if the “position” of the transition during odor morphing could be altered by training or by changing the olfactory environment after birth.

References

Abraham, N. M., H. Spors, et al. (2004). "Maintaining accuracy at the expense of speed: stimulus similarity defines odor discrimination time in mice." Neuron **44**(5): 865-76.

Barnes, D. C., R. D. Hofacer, et al. (2008). "Olfactory perceptual stability and discrimination." Nat Neurosci **11**(12): 1378-80.

Bathellier, B., D. L. Buhl, et al. (2008). "Dynamic ensemble odor coding in the mammalian olfactory bulb: sensory information at different timescales." Neuron **57**(4): 586-98.

Bozza, T., J. P. McGann, et al. (2004). "In vivo imaging of neuronal activity by targeted expression of a genetically encoded probe in the mouse." Neuron **42**(1): 9-21.

Brustein, E., N. Marandi, et al. (2003). ""In vivo" monitoring of neuronal network activity in zebrafish by two-photon Ca(2+) imaging." Pflugers Arch **446**(6): 766-73.

Carr, W. E. S. (1988). "The molecular nature of chemical stimuli in the aquatic environment." In: Atema J, Fay RR, Popper AN, Tavolga WN, editors. Sensory biology of aquatic animals. New York: Springer.: 3-27.

Cleland, T. A., B. A. Johnson, et al. (2007). "Relational representation in the olfactory system." Proc Natl Acad Sci U S A **104**(6): 1953-8.

Colgin, L. L., E. I. Moser, et al. (2008). "Understanding memory through hippocampal remapping." Trends Neurosci **31**(9): 469-77.

Cossart, R., D. Aronov, et al. (2003). "Attractor dynamics of network UP states in the neocortex." Nature **423**(6937): 283-8.

Denk, W., J. H. Strickler, et al. (1990). "Two-photon laser scanning fluorescence microscopy." Science **248**(4951): 73-6.

Dryer, L. and P. P. Graziadei (1994). "Mitral cell dendrites: a comparative approach." Anat Embryol (Berl) **189**(2): 91-106.

Fdez Galan, R., S. Sachse, et al. (2004). "Odor-driven attractor dynamics in the antennal lobe allow for simple and rapid olfactory pattern classification." Neural Comput **16**(5): 999-1012.

Finger, T. E. (1975). "The distribution of the olfactory tracts in the bullhead catfish, Ictalurus nebulosus." J Comp Neurol **161**(1): 125-41.

Firestein, S. (2001). "How the olfactory system makes sense of scents." Nature **413**(6852): 211-8.

Freeman, W. J. and K. A. Grajski (1987). "Relation of olfactory EEG to behavior: factor analysis." Behav Neurosci **101**(6): 766-77.

Friedrich, R. W., C. J. Habermann, et al. (2004). "Multiplexing using synchrony in the zebrafish olfactory bulb." Nat Neurosci **7**(8): 862-71.

Friedrich, R. W. and S. I. Korsching (1997). "Combinatorial and chemotopic odorant coding in the zebrafish olfactory bulb visualized by optical imaging." Neuron **18**(5): 737-52.

Friedrich, R. W. and S. I. Korsching (1998). "Chemotopic, combinatorial, and noncombinatorial odorant representations in the olfactory bulb revealed using a voltage-sensitive axon tracer." J Neurosci **18**(23): 9977-88.

Friedrich, R. W. and G. Laurent (2001). "Dynamic optimization of odor representations by slow temporal patterning of mitral cell activity." Science **291**(5505): 889-94.

Friedrich, R. W. and G. Laurent (2004). "Dynamics of olfactory bulb input and output activity during odor stimulation in zebrafish." J Neurophysiol **91**(6): 2658-69.

Gross-Isseroff, R. and D. Lancet (1988). "Concentration-dependent changes of perceived odor quality." Chemical Senses **13**(2): 191-204.

Haberly, L. B. (2001). "Parallel-distributed processing in olfactory cortex: new insights from morphological and physiological analysis of neuronal circuitry." Chem Senses **26**(5): 551-76.

Haberly, L. B. and J. L. Price (1977). "The axonal projection patterns of the mitral and tufted cells of the olfactory bulb in the rat." Brain Res **129**(1): 152-7.

Hasselmo, M. E., M. A. Wilson, et al. (1990). "Associative memory function in piriform (olfactory) cortex: computational modeling and neuropharmacology." Cold Spring Harb Symp Quant Biol **55**: 599-610.

Higashijima, S., M. A. Masino, et al. (2003). "Imaging neuronal activity during zebrafish behavior with a genetically encoded calcium indicator." J Neurophysiol **90**(6): 3986-97.

Hopfield, J. J. (1982). "Neural networks and physical systems with emergent collective computational abilities." Proc Natl Acad Sci U S A **79**(8): 2554-8.

Johnson, B. A. and M. Leon (2000). "Modular representations of odorants in the glomerular layer of the rat olfactory bulb and the effects of stimulus concentration." J Comp Neurol **422**(4): 496-509.

Khan, A. G., M. Thattai, et al. (2008). "Odor representations in the rat olfactory bulb change smoothly with morphing stimuli." Neuron **57**(4): 571-85.

Krone, D., M. Mannel, et al. (2001). "Qualitative and quantitative olfactometric evaluation of different concentrations of ethanol peppermint oil solutions." Phytother Res **15**(2): 135-8.

Laing, D. G., P. K. Legha, et al. (2003). "Relationship between molecular structure, concentration and odor qualities of oxygenated aliphatic molecules." Chem Senses **28**(1): 57-69.

Laurent, G., M. Stopfer, et al. (2001). "Odor encoding as an active, dynamical process: experiments, computation, and theory." Annu Rev Neurosci **24**: 263-97.

Leopold, D. A. and N. K. Logothetis (1999). "Multistable phenomena: changing views in perception." Trends Cogn Sci **3**(7): 254-264.

Leutgeb, J. K., S. Leutgeb, et al. (2005). "Progressive transformation of hippocampal neuronal representations in "morphed" environments." Neuron **48**(2): 345-58.

Levine, R. L. and S. Dethier (1985). "The connections between the olfactory bulb and the brain in the goldfish." J Comp Neurol **237**(4): 427-44.

Li, J., J. A. Mack, et al. (2005). "Early development of functional spatial maps in the zebrafish olfactory bulb." J Neurosci **25**(24): 5784-95.

Machens, C. K., R. Romo, et al. (2005). "Flexible control of mutual inhibition: a neural model of two-interval discrimination." Science **307**(5712): 1121-4.

Malnic, B., J. Hirono, et al. (1999). "Combinatorial receptor codes for odors." Cell **96**(5): 713-23.

Mathieson, W. B. and L. Maler (1988). "Morphological and electrophysiological properties of a novel in vitro preparation: the electrosensory lateral line lobe brain slice." J Comp Physiol [A] **163**(4): 489-506.

Mazor, O. and G. Laurent (2005). "Transient dynamics versus fixed points in odor representations by locust antennal lobe projection neurons." Neuron **48**(4): 661-73.

Meister, M. and T. Bonhoeffer (2001). "Tuning and topography in an odor map on the rat olfactory bulb." J Neurosci **21**(4): 1351-60.

Michel, W. C. and L. M. Lubomudrov (1995). "Specificity and sensitivity of the olfactory organ of the zebrafish, Danio rerio." J Comp Physiol A **177**(2): 191-9.

Miyawaki, A., J. Llopis, et al. (1997). "Fluorescent indicators for Ca2+ based on green fluorescent proteins and calmodulin." Nature **388**(6645): 882-7.

Mombaerts, P., F. Wang, et al. (1996). "Visualizing an olfactory sensory map." Cell **87**(4): 675-86.

Mori, K., Y. K. Takahashi, et al. (2006). "Maps of odorant molecular features in the Mammalian olfactory bulb." Physiol Rev **86**(2): 409-33.

Mozer, M. C. (2009). "Attractor Networks." P. Wilken, T. Bayne, & A. Cleeremans (Eds.), Oxford Companion to Consciousness. Oxford University Press.

Murphy, G. J., L. L. Glickfeld, et al. (2004). "Sensory neuron signaling to the brain: properties of transmitter release from olfactory nerve terminals." J Neurosci **24**(12): 3023-30.

Neville, K. R. and L. B. Haberly (2004). "Olfactory cortex. In: *The synaptic organization of the brain, Shepherd G. M. (ed)*." Oxford: Oxford University Press: 415-454.

Parker, A. J. and K. Krug (2003). "Neuronal mechanisms for the perception of ambiguous stimuli." Curr Opin Neurobiol **13**(4): 433-9.

Pologruto, T. A., B. L. Sabatini, et al. (2003). "ScanImage: flexible software for operating laser scanning microscopes." Biomed Eng Online **2**: 13.

Ressler, K. J., S. L. Sullivan, et al. (1994). "Information coding in the olfactory system: evidence for a stereotyped and highly organized epitope map in the olfactory bulb." Cell **79**(7): 1245-55.

Rink, E. and M. F. Wullimann (2004). "Connections of the ventral telencephalon (subpallium) in the zebrafish (Danio rerio)." Brain Res **1011**(2): 206-20.

Rotshtein, P., R. N. Henson, et al. (2005). "Morphing Marilyn into Maggie dissociates physical and identity face representations in the brain." Nat Neurosci **8**(1): 107-13.

Sachse, S. and C. G. Galizia (2003). "The coding of odour-intensity in the honeybee antennal lobe: local computation optimizes odour representation." Eur J Neurosci **18**(8): 2119-32.

Satou, M. (1990). "Synaptic organization, local neuronal circuitry, and functional segregation of the teleost olfactory bulb." Prog Neurobiol **34**(2): 115-42.

Scott, J. W., D. P. Wellis, et al. (1993). "Functional organization of the main olfactory bulb." Microsc Res Tech **24**(2): 142-56.

Shipley, M. T. and M. Ennis (1996). "Functional organization of olfactory system." J Neurobiol **30**(1): 123-76.

Stewart, W. B., J. S. Kauer, et al. (1979). "Functional organization of rat olfactory bulb analysed by the 2-deoxyglucose method." J Comp Neurol **185**(4): 715-34.

Stopfer, M., V. Jayaraman, et al. (2003). "Intensity versus identity coding in an olfactory system." Neuron **39**(6): 991-1004.

Stosiek, C., O. Garaschuk, et al. (2003). "In vivo two-photon calcium imaging of neuronal networks." Proc Natl Acad Sci U S A **100**(12): 7319-24.

Tabor, R., E. Yaksi, et al. (2004). "Processing of odor mixtures in the zebrafish olfactory bulb." J Neurosci **24**(29): 6611-20.

Taube, J. S. (1995). "Head direction cells recorded in the anterior thalamic nuclei of freely moving rats." J Neurosci **15**(1 Pt 1): 70-86.

Treves, A. and E. T. Rolls (1994). "Computational analysis of the role of the hippocampus in memory." Hippocampus **4**(3): 374-91.

Uchida, N. and Z. F. Mainen (2007). "Odor concentration invariance by chemical ratio coding." Front Syst Neurosci **1**: 3.

Uchida, N., Y. K. Takahashi, et al. (2000). "Odor maps in the mammalian olfactory bulb: domain organization and odorant structural features." Nat Neurosci **3**(10): 1035-43.

Valentincic, T., J. Kralj, et al. (2000). "The behavioral detection of binary mixtures of amino acids and their individual components by catfish." J Exp Biol **203**(Pt 21): 3307-17.

Valentincic, T., P. Miklavc, et al. (2005). "Correlations between olfactory discrimination, olfactory receptor neuron responses and chemotopy of amino acids in fishes." Chem Senses **30 Suppl 1**: i312-4.

Vassar, R., S. K. Chao, et al. (1994). "Topographic organization of sensory projections to the olfactory bulb." Cell **79**(6): 981-91.

von Bartheld, C. S., D. L. Meyer, et al. (1984). "Central connections of the olfactory bulb in the goldfish, Carassius auratus." Cell Tissue Res **238**(3): 475-87.

Wachowiak, M. and L. B. Cohen (2001). "Representation of odorants by receptor neuron input to the mouse olfactory bulb." Neuron **32**(4): 723-35.

Wachowiak, M., W. Denk, et al. (2004). "Functional organization of sensory input to the olfactory bulb glomerulus analyzed by two-photon calcium imaging." Proc Natl Acad Sci U S A **101**(24): 9097-102.

Wang, X. J. (2008). "Decision making in recurrent neuronal circuits." Neuron **60**(2): 215-34.

Wellis, D. P., J. W. Scott, et al. (1989). "Discrimination among odorants by single neurons of the rat olfactory bulb." J Neurophysiol **61**(6): 1161-77.

Wills, T. J., C. Lever, et al. (2005). "Attractor dynamics in the hippocampal representation of the local environment." Science **308**(5723): 873-6.

Wilson, D. A., M. Kadohisa, et al. (2006). "Cortical contributions to olfaction: plasticity and perception." Semin Cell Dev Biol **17**(4): 462-70.

Wullimann, M. F. and T. Mueller (2004). "Teleostean and mammalian forebrains contrasted: Evidence from genes to behavior." J Comp Neurol **475**(2): 143-62.

Xie, X., R. H. Hahnloser, et al. (2002). "Selectively grouping neurons in recurrent networks of lateral inhibition." Neural Comput **14**(11): 2627-46.

Yaksi, E. and R. W. Friedrich (2006). "Reconstruction of firing rate changes across neuronal populations by temporally deconvolved Ca2+ imaging." Nat Methods **3**(5): 377-83.

Yaksi, E., B. Judkewitz, et al. (2007). "Topological Reorganization of Odor Representations in the Olfactory Bulb." PLoS Biol **5**(7): e178.

Yaksi, E., F. von Saint Paul, et al. (2009). "Transformation of odor representations in target areas of the olfactory bulb." Nat Neurosci **12**(4): 474-82.

Acknowledgements

Curriculum Vitae

Personalien

Name:	Jörn Niessing
Privatadresse:	Kohlenberggasse. 23, 4051 Basel, Schweiz
Mobiltelefon:	0049-(0)179 949 10 72
Email:	Joern.niessing@gmail.com
Geburtstag & Ort:	28.02.1976, Marburg an der Lahn, Deutschland
Nationalität:	Deutsch
Zivilstand:	ledig, keine Kinder

Schul- & Berufsausbildung

2005 - 2010	**Doktorarbeit und Doktorprüfung: „summa cum laude“** (*Max-Planck Institute für medizinische Forschung*, Heidelberg / *Friedrich Miescher Institut für biomedizinische Forschung*, Basel, Schweiz). Unterstützt durch die *Studienstiftung des deutschen Volkes.* Beteiligte Dozenten: Dr. Rainer Friedrich, Prof. Andreas Lüthi und Prof. Silvia Arber.
Juli 2004	**Diplomarbeit und Diplomprüfung: „Mit Auszeichnung“** (*Max-Planck-Institut für Hirnforschung*, Frankfurt am Main, Betreuer: Prof. Dr. Wolf Singer
1998 – 2004	**Studium der Biologie** (Philipps-Universität Marburg / Johann Wolfgang Goethe Universität, Frankfurt am Main)
1997 – 1998	**Studium der Physik** (2 Semester, Philipps-Universität Marburg)
Juni 1997	**Abitur at Landschulheim Steinmühle**, Marburg
1990 – 1997	**Landschulheims Steinmühle**, Marburg
1989 – 1990	**Martin-Luther Gymnasiums**, Marburg
1983 – 1989	**Gebrüder-Grimm Grundschule**, Marburg

Ich erkläre, dass ich die Dissertation, “**Optophysiological analysis of pattern classification strategies in the zebrafish olfactory bulb”,** nur mit der darin angegeben Hilfe verfasst und bei kein anderen Fakultät eingereicht habe.